Stress-Induced Mucin 13 Reductions Drive Intestinal Microbiome Shifts and Despair Behaviors

Courtney R. Rivet-Noor[1,2,3], Andrea R. Merchak[1,2,3], Caroline Render[4], Naudia Gay[1,2,3], Rebecca M. Beiter[1,2,3], Ryan Brown[1,2,3], Austin Keeler[5], G. Brett Moreau[6], Sihan Li[2,7], Deniz E. Olgun[8,9], Alexandra D. Steigmeyer[10], Rachel Ofer[11], Tobey Mihn Huu Phan[9], Kiranmayi Vemuri[11], Lei Chen[12], Keira E. Mahoney[10], Jung-Bum Shin[2,7], Stacy A. Malaker[10], Chris Deppmann[5], Michael Verzi[10], and Alban Gaultier[1,2].

[1]Center for Brain Immunology and Glia, University of Virginia School of Medicine, Charlottesville, VA 22908, USA. [2]Department of Neuroscience, University of Virginia School of Medicine, Charlottesville, VA 22908, USA. [3]Graduate Program in Neuroscience, University of Virginia School of Medicine, Charlottesville, VA 22908, USA. [4]Undergraduate Department of Global Studies, University of Virginia College of Arts and Sciences, Charlottesville, VA, 22904, USA. [5]Department of Biology, University of Virginia College of Arts and Sciences, Charlottesville, VA, 22904, USA. [6]Division of Infectious Diseases and International Health, Department of Medicine, University of Virginia School of Medicine, Charlottesville, Virginia, USA. [7]Graduate Program in Biochemistry and Molecular Genetics, University of Virginia School of Medicine, Charlottesville, VA 22908, USA. [8]Undergraduate Department of Computer Science, University of Virginia School of Engineering and Applied Science, Charlottesville, VA 22904, USA. [9]Undergraduate Department of Neuroscience Studies, University of Virginia College of Arts and Sciences, Charlottesville, VA, 22904, USA. [10] Department of Chemistry, Yale University, New Haven, CT 06511, USA. [11] Department of Genetics, Human Genetics Institute of New Jersey, Rutgers Cancer Institute of New Jersey, Rutgers Center for Lipid Research, Division of Environmental & Population Health Biosciences, EOHSI, New Brunswick, New Jersey, 08901, USA. [12]School of Life Science and Technology, Key Laboratory of Developmental Genes and Human Disease, Southeast University, Nanjing, China.

Summary:

In this paper, authors identified a pathway by which stress induces microbiome shifts. They found that psychological stress selectively alters a key mucosal protein, mucin 13, which in turn modifies the microbial niche to induce changes in bacterial composition.

Abstract:

Depression is a prevalent psychological condition with limited treatment options. While its etiology is multifactorial, both chronic stress and changes in the microbiome are associated with disease pathology. In depression, stress is known to induce microbiome dysbiosis, defined here as a change in microbial composition associated with a pathological condition. This state of dysbiosis is then known to feedback on depressive symptoms. While studies have demonstrated that targeted restoration of the microbiome can alleviate depressive-like symptoms in mice, translating these findings to human patients has proven challenging due to the complexity of the human microbiome. As such, there is an urgent need to identify factors upstream of microbial dysbiosis. Here we investigate the role of mucin 13 as an upstream mediator of microbiome composition changes. Using a model of chronic stress, we show that the mucosal protein, mucin 13, is selectively reduced after psychological stress exposure. We further demonstrate that the reduction of *Muc13* is mediated by the *Hnf4* transcription factor family. Finally, we determine that deleting *Muc13* is sufficient to drive microbiome shifts and despair behaviors. These findings shed light on the mechanisms behind stress-induced microbial changes and reveal a regulator of mucin 13 expression.

48 **Introduction:**

49 Depression and anxiety impact millions of people worldwide.[1] Although many treatments
50 exist for these disorders, high rates of treatment-resistant cases remain, with up to 60% of
51 patients unable to find satisfactory results.[2] This large population of patients living without relief
52 for their mental health conditions highlights the need for further investigation into novel
53 therapeutic treatments. While the etiology of depression remains complex, stress is known to be
54 one of the largest contributing factors.[3,4] In addition, stress and depression are both associated
55 with changes in the gut microbiome.[5,6] Alterations in the gut microbiome composition are
56 present in depressed patients and conserved in animal models of depression, allowing
57 researchers to investigate the bacterial strains that are most associated with disease onset. The
58 microbiome has been extensively targeted as a potential treatment for mental health disorders:
59 modification of the microbiome has been shown to reduce depression symptoms in humans and
60 depressive-like behaviors in mice.[7-10] While promising, efforts to broadly manipulate the human
61 microbiome remain inconsistent due to the microbiome's complexity, unknown microbe-
62 microbe interactions, therapeutic microbes failing to colonize, microbe resource availability, and
63 host heterogeneity.[9,11,12] To circumvent current microbiome therapeutic limitations and increase
64 chances of successful microbial alterations in patients, there is a critical need to identify key
65 conserved, targetable regulators of the microbiome.

66 The mucosal layer is critical to maintaining both intestinal homeostasis and overall health.
67 In the absence of mucosal proteins, known as mucins, sweeping microbiome changes and
68 spontaneous disease occur.[13-17] Mucins are highly glycosylated proteins that fall into two
69 categories: soluble mucins and transmembrane mucins. [14,18] While soluble mucins make up the

70 gel-like layer that is commonly associated with mucus, transmembrane mucins remain tethered
71 to the cell membrane.[14,19] In the intestines, mucin 2 is the dominant soluble mucin, while mucin
72 13 and mucin 17 make up the majority of the intestinal transmembrane mucins (collectively
73 known as the glycocalyx).[14,19] Both soluble and transmembrane mucins have important roles in
74 regulating the intestine -- and importantly, the microbiome.[14] The mucosal layer provides both a
75 food source and anchor point for intestinal bacteria.[14] In addition, recent works have
76 demonstrated that the mucosal layer drives the stability and composition of the microbiome by
77 providing a permissive state for bacterial growth, and selecting for specific bacterial types along
78 the intestines by varying availability of glycan chains.[20-23] Supporting this idea, deletion of core 1
79 O-glycans in mice results in dramatic alterations to the microbiome composition and
80 spontaneous colitis.[24,25]

81 In addition, it has been demonstrated that stress hormones can alter the glycosylation
82 patterns of mucins, supporting the hypothesis that stress induces alterations in the mucosal layer
83 in a way that changes the microbial niche.[24,26,27] Together, these studies provide a foundation for
84 the hypothesis that stress can alter the mucus layer, and that this alteration can induce changes
85 in microbial composition.

86 Given the strong evidence supporting the role of the mucosal layer in microbiome
87 homeostasis and regulation, as well as the known ways in which stress can alter the mucosal
88 layer, we hypothesized that exposure to chronic stress alters the mucosal layer to change the
89 microbial niche and initiate microbiome changes. Here, we demonstrate that a model of chronic
90 stress selectively alters the expression of a transmembrane mucin, mucin 13. This change is not
91 seen after transfer of a microbiome from “stressed” mice into antibiotic treated or germ-free

92 mice, suggesting that changes in the microbiome composition itself does not reduce mucin 13.
93 In addition, we demonstrate the transcription factor hepatocyte nuclear factor 4 (HNF4)
94 regulates *Muc13* expression by binding the *Muc13* promoter. Finally, we demonstrate that
95 deletion of *Muc13* induces baseline despair behaviors, renders animals more susceptible to
96 anxiety-like behaviors, and alters microbial signatures in a way that mimics the composition of
97 microbes after stress exposure. Together, these findings suggest that Mucin 13 and HNF4 are
98 mechanistic regulators of stress-induced microbiome shifts.
99
100 **Results:**
101 **Unpredictable Chronic Mild Restraint Stress Drives Despair and Anxiety-Like Behaviors and**
102 **Modifies the Gut Microbiome Composition:**
103 To investigate the mechanisms of stress-induced microbiome alterations, we used
104 unpredictable chronic mild restraint stress (UCMRS), a version of a model of chronic stress known
105 to induce anxiety- and depressive-like behaviors and alter gut flora (Fig. 1A).[7] After three weeks,
106 mice exposed to UCMRS showed a significant increase in anxiety- like behaviors characterized by
107 an increase in nestlet shredding and decrease in time spent in the open arms of the elevated plus
108 maze (Fig. 1B). Despair behaviors were also detected through an increase in time inactive in both
109 the tail suspension and forced swim tests. In addition, a reduction in sucrose preference, a
110 measure for anhedonia, was observed in UCMRS exposed mice (Fig. 1B). In addition to behavioral
111 readouts, levels of murine stress-associated markers were measured from serum by mass
112 spectrometry (Fig. 1C and Ext. Data 1A-G). An increase in murine cortisol, but not corticosterone,
113 was detected in stressed mice, confirming a robust chronic stress response (Fig. 1C Ext. Data 1A).

114 While murine stress responses are often associated with changes in corticosterone, mice also
115 express cortisol to a lesser extent.[28-30] In addition, while changes in corticosterone are abundant
116 in acute models of stress, others have suggested that cortisol levels remain elevated in chronic
117 stress while corticosterone levels return to baseline.[28] Additionally, decreases in both serotonin
118 and glutamate were observed, consistent with findings in human depression.[31,32] No other
119 molecules tested were changed (Ext. Data 1A-G). This data highlights the validity of our model by
120 demonstrating that changes in molecules associated with human anxiety and depression, also
121 occur in mice exposed to UCMRS.

122 We next evaluated stress-induced microbiome composition changes by performing 16S
123 sequencing on fecal DNA from stressed and naïve animals. Using ASV-level data, we observed no
124 differences in measures of alpha diversity (richness (Fig. 1D) or evenness (Ext. Data 1H)).
125 However, there were significant differences in ASV-level derived beta diversity between naïve
126 and stressed animals (Fig. 1E). These differences were driven by changes in community
127 composition at the ASV level; for clarity, bacterial orders are depicted. Specifically, stress drove
128 relative reductions in *Clostridiales*, *Lactobacillales*, and an expansion of *Bacteroidales* (Fig. 1F and
129 Ext. Data 1I). Specific genus level changes between groups and the associated statistics can be
130 found in Ext. Data 1J and Ext. Data 5, Tab 2. Lastly, an ASV based random forest model accurately
131 predicted the bacterial orders associated with either baseline or stressed groups, strengthening
132 the link between stress and specific microbial shifts (Fig. 1G). Taken together, these results
133 demonstrate that unpredictable chronic mild restraint stress (UCMRS) induces despair and
134 anxiety-like behaviors in mice, alters murine stress hormone levels, and induces composition
135 shifts in the murine microbiome.

136

137 **Unpredictable Chronic Mild Restraint Stress Reduces *Muc13* Expression *In Vivo*:**

138 While it is well accepted that stress can change the microbiome in humans and mice (Fig.
139 1), the mechanisms behind these microbial shifts remain unknown.[9,33-36] Because the mucosal
140 layer, primarily composed of heavily glycosylated mucins, provides both an anchor point and
141 nutrient reservoir for bacteria, we hypothesized that a change in mucin composition could induce
142 microbiome shifts.[18,19,37] To test this, we first evaluated if mucin expression changed in stressed
143 conditions. Using RNA extracted from individual sections of the intestines of mice exposed to
144 UCMRS and naïve controls (Fig. 2A), we examined mucin expression by qPCR. Of all the mucins
145 examined (all detectable mucins: *Muc1*, *2*, *4*, *13*, and *17*), we found that *Muc13* was uniquely
146 reduced across intestinal segments (Fig. 2B-C and Ext. Data 2A-C). Additionally, to examine mucin
147 changes across genetic background, we examined *Muc13* and *Muc2* expression in BALB/cJ mice
148 exposed to stress. We found a similar reduction in *Muc13*, while no changes in *Muc2* expression
149 were observed (Ext. Data 2D-E). Taken together, these results suggest that stress induces changes
150 in *Muc13* expression, and that these changes are conserved across different genetic
151 backgrounds.

152

153 **Stress-Induced *Muc13* Reductions are Driven Independently of Transferrable Microbial**
154 **Products:**

155 The microbiome is a known influencer of the mucus layer. While we hypothesized that
156 stress-induced changes in the mucosal layer lead to changes in microbiome composition, we also
157 considered that stress-induced shifts in the microbiome could instead be modulating *Muc13*

158 expression.[37,38] If this was the case, it would suggest that mucin 13 changes would occur after
159 microbial shifts in our model. To test this hypothesis, we utilized two different models to examine
160 the impacts of the microbiome on mucin 13. First, after treating mice with antibiotics for two
161 weeks, we transferred the fecal microbiomes from naïve or stressed mice via oral gavage (Fig.
162 2D). Two weeks post reconstitution, intestinal samples were collected to examine microbiome
163 composition and mucin expression. 16S sequencing revealed that donor samples clustered
164 distinctly from each other (Ext. Data 2F, light blue and dark pink). In addition, recipient mice
165 clustered nearer to their donor sample but separately from each other, demonstrating distinct
166 microbiomes and successful transfer of the expected signatures (Ext. Data 2F-G). We next
167 examined RNA expression of intestinal mucins between groups. Importantly, no change in mucin
168 13 expression was detected between animals that received a stressed or naïve microbiome (Fig.
169 2E). In addition, we saw no change in any other mucins expressed between groups (Fig. 2F and
170 Ext. Data 2H-J). These data demonstrate that microbial signatures from the transferred stressed
171 microbiomes are not sufficient to reduce mucin 13 expression.

172 To complement this approach, we also examined the impact of stressed microbial
173 signatures in germ free mice. Our lab has successfully demonstrated that microbial signatures
174 from stressed mice can alter despair and anxiety-like behaviors in germ free mice.[39] Therefore,
175 using intestinal samples collected from germ free mice which were given fecal pellets from naïve
176 or stress-exposed animals, we again examined changes in mucin expression by qPCR. Our results
177 indicated that, similar to the antibiotic treated mice, no reduction in *Muc13* was observed (Fig.
178 2G). While we saw no changes in *Muc1*, *Muc4*, or *Muc17*, we did see an expected increase in
179 *Muc*2 expression with microbiome reconstitution in germ free mice (Fig. 2H and Ext. Data 2K-

180 M).[40] These results demonstrate that microbial signatures from stressed animals, while enough
181 to induce behavioral changes, are not sufficient to reduce *Muc13* expression in the intestines.
182 This again suggests that the mucin 13 changes observed in stress are not driven by -- and indeed
183 likely precede -- microbial changes in the intestines. Taken together, these results support the
184 hypothesis that stress-induced reductions in mucin 13 are driven independently of transferrable
185 microbial signatures.
186
187 ***Muc13* Reductions are Driven by Reductions in Intestinal HNF4:**
188 To understand how stress induces reductions in *Muc13* expression, we explored
189 transcription factors which are known to bind to *Muc13* by examining published small intestine
190 and colon ChIP-seq data sets through the UCSC genome browser.[41] Results revealed that
191 hepatocyte nuclear factor 4 (HNF4) is able to bind to the promoter region of *Muc13* in both the
192 small and large intestines.[42,43] HNF4, a transcription factor which is a member of the nuclear
193 receptor superfamily, plays a critical role in regulating metabolism, epithelial tight junctions, and
194 the differentiation and proliferation of enterocytes in the intestines.[44] In addition to these
195 functions, *Hnf*4 expression has been shown to regulate the brush border, the collection of
196 microvilli along the intestinal tract.[45] As the brush border is thought to be modulated by the
197 density of the glycocalyx, and therefore transmembrane mucins, HNF4 is a logical candidate to
198 mediate changes in *Muc13* expression.[46] Importantly, stress hormones have also been shown to
199 inhibit *Hnf*4 expression in a model of high fat diet.[47] Together, these works provide a foundation
200 for the hypothesis that stress may be able to regulate *Hnf4* expression in a way that reduces
201 *Muc13* expression.

202 In order to investigate the ability of HNF4 to regulate *Muc13* expression, we first analyzed
203 previously performed HNF4 and H3K27ac ChIP-seq on wildtype duodenal villus cells to examine
204 binding at the *Muc1*3 locus.[48] Results indicated that in wildtype mice, both HNF4 and H3K27ac, a
205 marker of transcription, are enriched in the promoter region of *Muc13* (Fig. 3A). This suggests
206 that HNF4 binds the *Muc13* promoter in a site that is marked for active transcription, supporting
207 the idea that HNF4 can regulate *Muc13* expression. We next wanted to examine the impacts of
208 HNF4 deletion on *Muc13* expression in the intestine. To do this, we utilized the previously
209 described *Villin-Cre*^{ERT2}; *Hnf4a*$^{F/F}$; *Hnf4g* $^{Crispr/Crispr}$ double knockout mouse line (*Hnf4* DKO) which
210 lacks both HNF4 paralogs.[48] Analyzing previously performed RNA Polymerase II (RNAP2) ChIP-seq
211 on duodenal villus epithelial cells in wildtype controls and *Hnf4* DKO animals, we found that the
212 RNAP2 signal at the *Muc13* promoter is markedly reduced in the *Hnf4* DKO animals compared to
213 controls (Fig. 3B). To complement this approach, we further examined previously performed
214 H3K4me3 chromosome conformation capture with chromatin immunoprecipitation (HiChIP) and
215 RNA-seq on control and *Hnf4* DKO duodenal villus epithelial cells.[49] Analysis revealed fewer
216 H3K4me3 chromatin loops in the *Muc13* promoter region in *Hnf4* DKO animals than in control
217 duodenal villus epithelial cells, suggesting fewer sites of active transcription (Fig. 3C). In addition,
218 RNA sequencing results showed a significant reduction in *Muc13* expression in duodenal villus
219 epithelial cells after the loss of *Hnf4* (Fig. 3D). We next performed qPCR for mucin expression on
220 all sections of the intestines from control and *Hnf4* DKO animals. We found that in addition to
221 the successful deletion of the *Hnf4* paralogs (Fig. 3E-F), there was also a significant reduction in
222 *Muc13* expression across the intestines (Fig. 3G), that was not seen in any other tested mucins
223 (Fig 3H and Ext. Data 3A). Lastly, we analyzed intestinal expression of *Hnf4* from mice exposed to

224 3 weeks of UCMRS (Fig. 1A). Our results indicated that *Hnf4* expression is significantly reduced
225 in the intestines after stress exposure (Fig. 3I-J). In addition, leucine rich repeat containing G
226 protein coupled receptor 5 (Lgr5), which is known to be suppressed in *Hnf4* knockout animals,
227 was also significantly reduced (Fig. 3K).[50] Furthermore, germ-free mice that had been given fecal
228 pellets from stressed or naïve mice showed no differences in *Hnf4* expression, suggesting that
229 *Hnf4* expression is not driven by transferrable microbial products (Ext. Data 3B-C).

230 In order to examine the impacts of HNF4 on *Muc13* expression more directly, we utilized
231 HT-29 cells. HT-29 cells are a human colon cancer cell line that is known to express both mucins
232 and *Hnf4*.[51,52] Cells were treated with an HNF4 antagonist (BI6015) or a DMSO control for 24
233 hours.[53,54] We then extracted the RNA from the collected cells and examined mucin expression
234 as before. We found that treatment with the antagonist BI6015 showed a significant
235 downregulation of *MUC13* expression (Fig. 3L). In addition, *LGR5* showed decreased expression
236 with BI6015, demonstrating successful antagonist activity on HNF4 (Fig. 3M).[50] Finally, BI6015
237 was also found to significantly decrease expression of *MUC1* and significantly increase expression
238 of *MUC17* (Fig. 3N-O). However, as the expression of these other transmembrane mucins was
239 not impacted by HNF4 reductions *in vivo* (Ext. Data 2B-C, Ext. Data3A), there are likely other
240 factors that more strongly contribute to changes in their expression. These results further
241 support the hypothesis that *MUC13* is regulated by HNF4.

242 Together, these data suggest that in the absence of HNF4, there is less active
243 transcription at, and fewer transcripts of, the *Muc13* gene; this supports the hypothesis that
244 *Muc13* is regulated by HNF4. Our results also demonstrate that after UCMRS exposure, there is
245 a significant reduction in *Hnf4* that occurs independently of transferrable microbial products,

246 suggesting that stress is capable of reducing *Hnf4 in vivo*. Finally, we show that direct modulation
247 of HNF4 results in *Muc13* expression changes *in vitro,* validating our *in vivo* findings. Taken
248 together, these results demonstrate that *Muc13* expression is modulated by HNF4 both *in vitro*
249 and *in vivo,* and after stress exposure.
250
251 ***Muc13* Deletion Induces Baseline Behavioral and Microbiome Changes and Renders Mice More**
252 **Susceptible to UCMRS:**
253 Given our data demonstrating that *Muc13* is specifically downregulated in stressed
254 animals (Fig. 2B), we sought to examine if deleting *Muc13* impacted the microbiome and
255 behavioral outputs in mice. Using the *i*-GONAD system, we created a *Muc13* knockout (*Muc13*$^{-/-}$
256) mouse line by deleting a 475bp region of the *Muc13* gene containing the start codon (Fig.
257 4A).[55,56] Validation of the knockout line was performed using both qPCR (Fig. 4B-C) and
258 immunofluorescence (Fig. 4D-E). Importantly, no changes were observed in *Muc2* at the
259 transcript or protein levels, suggesting that *Muc2* expression was not changed with the loss of
260 *Muc13* (Fig. 4C and F). To complement this approach, we also examined detectable mucins at the
261 protein level by mass spectrometry in *Muc13*$^{-/-}$ and control animals. To do this, we employed a
262 mucin enrichment strategy that takes advantage of an inactive protease selective for mucin
263 domains; mucins from *Muc13*$^{-/-}$ and control animal intestines were enriched and subjected to MS
264 analysis.[57,58] We were able to see a significant reduction in the MUC13 protein in all sections of
265 the intestine (Fig. 4G). No other detectable mucin was statistically significantly changed (Fold
266 Change >5), suggesting that none of the other membrane mucins nor soluble mucins,

267 compensate for the loss of MUC13. Together, these data demonstrate a successful deletion of
268 MUC13 in our knockout line.

269 We next sought to understand the impacts of *Muc13* deletion on microbiome
270 composition. We compared 16S sequencing results from fecal samples collected from adult
271 wildtype and *Muc13*$^{-/-}$ animals that were separated by genotype at weaning. Interestingly, we
272 found that *Muc13*$^{-/-}$ animals (light green) clustered distinctly from wildtype controls (light
273 orange), suggesting that *Muc13* deletion significantly impacts the composition of the microbiome
274 at baseline (Fig. 5B). In addition, to understand if *Muc13*$^{-/-}$ animals have stress induced
275 microbiome shifts, we used an abbreviated 1-week UCMRS protocol (Fig. 5A). In our hands, this
276 abbreviated protocol allows for substantial microbial shifts, but does not yet yield all stress-
277 induced anxiety-like and despair behaviors in wildtype animals (Fig. 5D-G, light orange to dark
278 pink bars). This allows us to examine if *Muc13*$^{-/-}$ animals are susceptible to different UCMRS
279 induced microbial shifts than wildtype controls, and if *Muc13*$^{-/-}$ mice are more susceptible to
280 UCMRS-induced behavioral changes. Our results show that while wildtype samples show a
281 significant shift in microbial composition after 1 week of UCMRS (light orange to dark pink dots),
282 *Muc13*$^{-/-}$ (light green to dark green dots) samples remained clustered together (Fig. 5B). This
283 suggests that the microbiome of *Muc13*$^{-/-}$ animals is different from WT animals at baseline and
284 is less modified by 1-week of UCMRS exposure. In addition, samples from wildtype animals
285 exposed to 1 week of UCMRS shifted towards both groups (baseline and 1 week UCMRS, light
286 and dark green dots) of the *Muc13*$^{-/-}$ animals, supporting the idea the *Muc13*$^{-/-}$ animals have
287 microbial signatures which mimic stress-induced microbiome signatures (Fig. 5B). To further
288 understand the similarities between the *Muc13*$^{-/-}$ microbiome and the UCMRS-exposed

289 microbiome, we compared the significantly changed bacterial families between baseline
290 wildtype and baseline *Muc13*$^{-/-}$ animals to the significantly changed bacterial families between
291 baseline wildtype animals and wildtype animals exposed to 1 week of UCMRS. Of the bacterial
292 families that had significant changes in either group, 69% of those changes overlapped (Fig. 5C).
293 While we also examined overlapping changes at the genus and ASV levels, algorithm matching
294 limitations hindered our ability to draw conclusions. While 58% of genera and 62% of ASV
295 changes overlapped between groups, only ~45% of total reads could be matched to a known
296 genus or ASV -- making clear comparisons at these levels difficult (Ext. Data 5, Tab 3).
297 Nonetheless, data at the family level suggests significant overlap in changes between baseline
298 control and baseline *Muc13*$^{-/-}$ animals when compared to baseline control and UCMRS exposed
299 controls. Together, these data further suggest that *Muc13* deletion induces a change in the
300 microbiome that closely mimics the microbial shifts observed after UCMRS exposure.

301 Given the established connection between microbiome changes and mental health, we
302 sought to examine if *Muc13* deletion impacted anxiety-like and despair behaviors in mice.[7] Both
303 *Muc13*$^{-/-}$ animals and wildtype controls were subjected to the open field, nestlet shred, tail
304 suspension, and forced swim tests (Fig. 5A, D-G). Behavior was collected at baseline and after 1
305 week of UCMRS for all animals. Interestingly, at baseline, we observed no differences in anxiety-
306 like behaviors in the open field or nestlet shredding tests between *Muc13*$^{-/-}$ and wildtype controls
307 (Fig. 5D-E, left columns). However, strong despair behaviors were observed in both the tail
308 suspension and forced swim tests (Fig. 5F-G, left columns), suggesting *Muc13*$^{-/-}$ mice display
309 innate despair, but not anxiety-like, behaviors. In addition, to gain a full picture of the impact of
310 *Muc13* deletion on susceptibility to stress-induced despair and anxiety-like behaviors, we

311 subjected wildtype and *Muc13*$^{-/-}$ mice to 1 week of UCMRS. Critically, as supported by other
312 studies, 1 week of UCMRS exposure represents a subclinical model of stress that does not induce
313 all expected behavioral changes in wildtype animals[59,60]. Thus, we hypothesized that if *Muc13*$^{-/-}$
314 deletion rendered animals more susceptible to stress, they would exhibit despair and anxiety-
315 like behaviors earlier than wildtype animals.[61] Supporting this hypothesis, following 1 week of
316 UMCRS, *Muc13*$^{-/-}$ animals had significant reductions in the amount of time spent in the center of
317 the open field test, as well as significant increases in the amount of nestlet removed in the nestlet
318 shred test. These results indicate that 1 week of UCMRS is sufficient to induce anxiety-like
319 phenotypes in *Muc13*$^{-/-}$ animals, but not their wildtype counterparts (Fig. 5D-E, green columns).
320 Furthermore, in the tail suspension and forced swim tests, we saw no increase in time spent
321 inactive as the *Muc13*$^{-/-}$ animals presented with despair behaviors at baseline and likely hit a
322 ceiling effect (Fig. 5F-G, green columns). To complement these classical behavioral assays, we
323 used unbiased artificial intelligence (DeepLabCut) to detect animal poses (Fig. 5H-J and Ext. Data
324 4).[62,63] In this approach, 10-minute videos of mice exploring an open field box were broken down
325 into 25 individual motifs (Fig. 5H). Each motif was characterized and grouped into a general
326 behavioral classification (rearing/grooming, turning, etc.). Individual motifs represent a
327 behavioral pattern based on mouse limb and tail position detected by DeepLabCut. For example,
328 the general behavior classification "turning" included motifs such "head turning left", "mid-point
329 of right turn", etc. As these motifs all make up a complete behavior, there were grouped in
330 general classifications. Once grouped, changes in the percentage of time spent in each behavioral
331 motif were quantified between *Muc13*$^{-/-}$ and wildtype animals (Fig. 5H-J). Baseline analysis
332 revealed that of the 25 distinct motifs, 16% were significantly changed between groups (Ext. Data

333 4A-B), suggesting that, like in classical behavioral assays, distinctions between *Muc13*$^{-/-}$ and
334 wildtype animals are present at baseline. Similarly, the DeepLabCut software was able to detect
335 significant differences between groups after 1 week of UCMRS exposure, with 40% of behavioral
336 motifs being changed between *Muc13*$^{-/-}$ and wildtype controls (Fig. 4I-J).

337 Our results show that *Muc13* deletion can drive both microbiome shifts that mirror
338 microbial changes induced by stress, and despair behaviors at baseline -- highlighting the critical
339 role of mucin 13 in maintaining microbial and behavioral homeostasis. In addition, deletion of
340 *Muc13* renders animals more susceptible to stress-induced anxiety-like behaviors. Together,
341 these results support the hypothesis that stress induced *Muc13* reductions can drive microbial
342 shifts that lead to behavioral changes in mice.

343

344 **Discussion:**

345 Our work demonstrates that stress induces microbiome changes and behavioral changes
346 in mice. In addition, stress also reduces expression of a key component of the mucosal layer,
347 mucin 13. Our data also supports the hypothesis that stress mediates this reduction in *Muc13*
348 expression by reducing the intestinal transcription factor HNF4. Furthermore, we demonstrate
349 that deletion of mucin 13 is sufficient to induce microbiome shifts and behavioral changes that
350 mimic stress-induced phenotypes at baseline. In addition to these baseline changes, mice lacking
351 mucin 13 also are more susceptible to behavioral changes after exposure to a model of sub-
352 clinical unpredictable chronic mild restraint stress. Together, these data define how stress is able
353 to induce shifts in microbial composition in the intestines, providing a foundation for future
354 studies.

355 Our results are supported by concepts in previously published literature. For example, it
356 is well known that there is a reciprocal relationship between the mucus layer and microbes.[37] In
357 fact, disruption of the intestinal mucus layer results in sweeping microbiome changes,
358 heightened inflammation, and disease onset-- supporting the idea that changes in mucus can
359 impact other systems in the body.[13,16,17,37,64-68] Additionally, stress has been shown to alter the
360 glycosylation patterns of mucins.[27] As changes in glycosylation are also known to alter the
361 microbiome, the connection between stress and mucin induced microbiome changes is well
362 supported.[23,69] Finally, the connection between mucins and depression has also been suggested
363 in the literature. Specifically, single nucleotide polymorphisms (SNPs) in *MUC13* have been
364 identified in GWAS studies of depressed populations.[70-72] In addition, SNPs in O-glycosylation
365 have also been identified in populations with treatment resistant depression.[72,73] In aggregate,
366 these data support our results, suggesting that mucin 13 is an important driver of microbiome
367 shifts and despair behaviors in mice.

368 Mechanistically, our results show that HNF4 can bind to the *Muc13* promoter, while the
369 loss of *Hnf4* results in reduced transcription of *Muc13* in the intestines of mice. In addition, we
370 have shown that chronic stress induces reductions in both *Muc13* and *Hnf4* expression. While
371 more work is needed to understand how stress regulates *Hnf4* in our chronic stress model,
372 literature suggests that this regulation could occur through the phosphorylation of extracellular
373 signal-regulated kinase (ERK) 1/2. While there is no glucocorticoid response element (GRE) in the
374 *Hnf4* gene, ERK 1/2 is known to be a potent inhibitor of *Hnf4* expression.[74] In addition, stress
375 hormones have repeatedly been demonstrated to enhance ERK 1/2 phosphorylation.[75-77] These
376 works provide a mechanistic foundation for how stress could be reducing *Hnf4* expression in the

377 intestines. While the basis for our hypothesis is well supported, no works have demonstrated
378 how stress specifically regulates *Hnf4*, leaving a gap in knowledge to be filled by future studies.
379 By defining a novel mechanism through which stress alters the microbiome, our results
380 have brought to light a key aspect in stress-induced behavioral changes. We have demonstrated
381 that a transmembrane mucin is specifically and indirectly regulated by stress in a way that
382 interferes with its homeostatic expression patterns, inducing microbiome composition changes
383 and despair behaviors in mice. Mucin 13 is conserved between humans and mice, meaning that
384 it could be a broadly applicable therapeutic target for patients with stress-induced depression,
385 who present with microbiome changes. Although our results are directly related to stress-
386 induced depression, they provide a basis for further research to target transmembrane mucins
387 as intervention points for diseases that present with or are driven by pathogenic microbiome
388 alterations, such as colitis or Parkinson's Disease.[78]
389
390 **Methods**
391 ***Mice:*** C57BL/6j and BALB/cJ mice were purchased from Jackson Laboratories (strain #000664 and
392 #000651, respectively). Mice were bred in-house and kept on a 12-h light/dark schedule. All mice
393 were group housed up to 5 mice per cage unless separated for fighting or designated to a stressed
394 group, where they were singly housed. All behavioral interventions were performed between 8
395 am and 3 pm and animals were sacrificed between 7 am and 1 pm. Experimental and control
396 animals were sacrificed in alternating patterns to ensure proper controls for circadian
397 consideration. *Villin-Cre*^{ERT2}; *Hnf4a*$^{F/F}$; *Hnf4g*$^{Crispr/Crispr}$ animals were generated at Rutgers
398 University under the care of the Verzi lab. Inducible knockouts for sequencing were given 1

399 injection of tamoxifen (50mg/kg) for 2-3 days (2-3 total doses) to catch early changes in the
400 intestines. HNF4 DKO mice used for qPCR were given 1 injection of tamoxifen (50mg/kg) for 4
401 days (4 total doses). Animals were harvested on the 5th day. All control animals were given saline.
402 Mucin-13 knockout lines were generated using the iGONAD technique as described, using
403 a BTX ECM 830 Electroporation System (Harvard Apparatus).[55,56] Briefly, the *Muc13* sequence
404 was taken from the UCSC genome browser, mouse assembly Dec. 2011 (GRCm38/mm10),
405 Genomic Sequence (chr16:33,794,037-33,819,927)[41]. Exons 1 and 2 including the intervening
406 intron where analyzed with CRISPOR (http://crispor.tefor.net/; Concordet and Haeussler 2018)[93].
407 Exon 2, containing the protein start sequence, was targeted for excision at these two target
408 sequences + PAM sites: Exon2_protein_start_sequence GCAAGAGCAGCTACCATGAA (AGG) and
409 Exon2_end_of_exon AGTCTCCTTTTGGTGACCGT (GGG). Alt-R S.p. HiFi Cas9 Nuclease, tracrRNA,
410 and crRNA XT for the two target sequences were purchased (IDT). Prior to surgery, the Alt-R
411 CRISPR/Cas9 reagents were prepared according to IDT guidelines: crRNA-XT and tracrRNA were
412 annealed to form the gRNA, then complexed to the S.p HiFi Cas9 nuclease, and then diluted with
413 sterile Opti-MEM with Fast Green FCF to aid visualization.
414 Plugged females were anesthetized and maintained with isoflurane ~16 hours after
415 copulation was assumed to have occurred (estimate copulation around midnight, surgeries were
416 done at 4pm). Anesthesia was confirmed by toe pinch and eyes were lubricated with Puralube
417 ointment. The lower dorsal skin of the mouse was soaked in betadine followed by two washes
418 with isopropanol. A dorsal incision was made to expose the ovaries, oviduct, and uterine horn.
419 Using a pulled micropipette, ~1.5ul of the CRISPR/Cas9 solution was drawn up and then injected
420 between the infundibulum and ampulla, intraoviductally dispensing the solution slowly to avoid

421 backflow. The oviduct was covered in a wetted, sterile kimwipe and immediately electroporated
422 using 3-mm platinum tweezer rode electrodes (BTX) delivering 50V for 5ms with 1s interval for 8
423 square-wave pulses using a BTX ECM 830 Electroporation System (Harvard Apparatus). The
424 oviduct was returned to the abdominal cavity and the procedure was repeated on the opposite
425 side oviduct. Once both oviducts were injected and electroporated the incision was sutured, and
426 the stitches secured with liquid bandage before receiving a postop subcutaneous injection of
427 ketoprofen (5mg/kg of mouse body weight) with subsequent injections for up to five days as
428 needed. All procedures were approved by the University of Virginia ACUC (protocol #3918). All
429 experiments were conducted and reported according to ARRIVE guidelines.
430

431 **METHOD DETAILS**

432 ***Stress Experiments and Behavioral Tests:*** Unpredictable Chronic Mild Restraint Stress (UCMRS)
433 experiments and behavioral experiments (the forced swim, tail suspension, sucrose preference,
434 open field, elevated plus maze, and nestlet shred tests) were performed as previously
435 described.[62]

436 ***Stress protocol:*** For UCMRS, all animals were single housed. Mice were exposed to 2
437 hours of restraint stress and one overnight stressor per day. Restraint stress was performed by
438 putting mice into ventilated 50mL conical tubes for 2 hours. Overnight stressors included one of
439 the following: 45-degree cage tilt, wet bedding, or 2x cage change. Wet bedding was performed
440 by wetting standard cage bedding with ~200mL of murine drinking water. 2x cage change

441 included replacing cage bases 2x within 24 hours. 45-degree cage tilt included propping cages up
442 to ~45-degrees overnight.

443 ***Behavioral Tests:*** All testing (with exception to the nestlet shred and sucrose preference
444 tests) was recorded on a Hero Session 5 GoPro and analyzed with Noldus behavioral analysis
445 software.

446 *Nestlet Shred:* Mice were moved into fresh individual cages and allowed to habituate for
447 1 hour. After 1 hour, a weighed nestlet was placed in the center of the cage. Mice were allowed
448 to interact with the nestlet for 30 min. After 30 min, nestlets were removed and weighed. Before
449 weighing, excess nestlet was stripped from the main piece of nestlet by lightly dragging fingers
450 across each area of the nestlet starting from the center (center up, center left, center right, center
451 down). Once completed, nestlet was flipped and the process was repeated for the corners (center
452 to upper right, center to upper left, center to lower right, center to lower left). Equal pressure
453 was applied to each nestlet. Change in amount shredded and percent shredded were calculated
454 from the weighed nestlet values.

455 *Sucrose Preference test:* Mice were housed individually and given 2 water bottles/cage.
456 One water bottle contained normal drinking water, the other contained 1% sucrose water. Mice
457 had access to the bottles for 3 days. On Day 0, bottles were primed and weighed and put in cages.
458 Day 1: 24 hours later, water bottles were removed from cages and weighed. Once weighed,
459 bottles were replaced, but with swapped positions (i.e.- if sucrose was on the left on Day 0, it was
460 on the right on Day 1). The first night of sucrose preference is considered habituation and the
461 values are not included in analysis. Day 2: 24 hours after replacing water bottles, bottles were

462 weighed and replaced as on day 1. Day 3: 24 hours after replacing water bottles, bottles were
463 removed and weighed for a final time. Sucrose preference was calculated by determining the
464 percentage of each bottle drunk on day 2 and 3 and averaging those values.

465 *Elevated Plus Maze:* Mice were placed on an elevated plus maze apparatus and allowed
466 to explore for 5 minutes. The elevated plus maze was cleaned with 70% ethanol between each
467 run and recorded on a GoPro Hero Session 5 or 8. Files were analyzed with Noldus behavior
468 software.

469 *Open field/DeepLabCut:* Animals were placed into a 14in x 14in box with opaque walls
470 and a raised clear bottom (18in). Animals were allowed to explore freely for 10 minutes. Hero
471 session 8s were placed ~18in below the box to record animal movements from below. Noldus
472 behavioral software was used to determine if animals were in the perimeter or center of the box.
473 Videos were also used for DeepLabCut analysis. Analysis is described below.

474 ***Metabolite Mass Spectrometry:*** 25 µL of plasma was extracted using 500 µL of cold
475 acetonitrile followed by vortexing and 10 minutes of centrifugation at 14K rpm. 450 µL of the
476 resulting supernatant was transferred to a clean Eppendorf and dried completely by Speedvac.
477 Each sample was reconstituted with 25 µL of 50% methanol in 0.1% formic acid/water, vortexed
478 and transferred to autosampler vials for analysis by mass spectrometry. Eleven metabolites were
479 quantitated by PRM (parallel reaction monitoring) using a Thermo Orbitrap ID-X mass
480 spectrometer coupled to a Waters BEH C18 column (15 cm x 2.1 mm). Metabolites were eluted
481 with a Vanquish UHPLC system over a 15 min gradient (10 µL injection, 200 µL/min, buffer A –

482 0.1% formic acid in water, buffer B - 0.1% formic acid in methanol). The mass resolution was set
483 to 120K for detection using the transitions outlines in Extended Data 5, Tab 1.
484 Raw data files for samples, blanks and calibration curves were imported into Skyline
485 (https://skyline.ms/project/home/begin.view). Calibration curves were generated with a linear
486 regression. Peak areas for analytes in samples were used for quantification based in the
487 generated calibration curves. Raw files can be downloaded for analysis at
488 https://www.metabolomicsworkbench.org under study ID: ST002345
489
490 ***Mass Spectrometry:*** Frozen intestinal tissue sections were homogenized use the Cryo-
491 Cup Grinder (BioSpec Products, Cat. No. 206) according to manufacturer's instructions.
492 Pulverized tissue was transferred into ice-cold 150 uL dialyzable lysis buffer, consisting of 1% N-
493 octylglucoside (Research Products International, N02007), 1% CHAPS (Research Products
494 International, C41010), 50 mM Tris (American Bio, AB14044), 100 mM NaCl (Research Products
495 International, S23025), 2 mM $MgCl_2$ (American Bio, AB09006), benzonase (Sigma Aldrich, E1014),
496 and protease inhibitor (Roche, 11836170001). Samples were rotated at 4 °C for 2 hours, followed
497 by centrifugation for 30 minutes at 15,000 rcf and passed through a 0.7 µm filter. StcE^{E447D} was
498 expressed and purified as previously described.[57,58] 500 ug of NHS-Activated Agarose Slurry
499 (Thermo Fisher Scientific, 26200) was activated with 1 mM HCl and PBS. StcE^{E447D} (1 mL of 1.45
500 mg/mL) was added to the slurry and rotated at 4 °C for 3 hours. Beads were rinsed with 100 mM
501 Tris and the reaction quenched with 100 mM acetate buffer. Beads were washed with 20 mM
502 Tris. Beads were then washed and stored in 20 mM Tris 150 mM NaCl. Filtered supernatants were
503 rotated overnight at 4 °C with 100 uL StcE^{E447D}-NHS bead slurry and 0.01 M EDTA. All reactions

504 were brought up to 1 mL with 20 mM Tris 150 mM NaCl. Beads were then rinsed with 10 mM Tris
505 1 M NaCl, 10 mM Tris 150 mM NaCl, 10 mM NaCl and MS grade water (Thermo Scientific, 51140).
506 Protein was eluted with 1% sodium deoxycholate (Research Products International, D91500-
507 25.0) in 50 mM Ammonium bicarbonate (AmBic) (Honeywell Fluka, 40867), at 95 °C for 5 minutes.
508 Dithiothreitol (DTT) (Sigma Aldrich, D0632) was added to 20% of the eluent to a final
509 concentration of 2mM and allowed to react at 65 °C for 25 minutes. Alkylation in 5 mM
510 iodoacetamide (IAA) (Sigma Aldrich, I1149) was performed for 15 minutes in the dark at room
511 temperature. 0.05µg of sequencing-grade trypsin (Promega, V5111) was added to each 20%
512 aliquot and allowed to react for 3 hours at 37 °C. Reactions were quenched by adding 1 µL formic
513 acid. All reactions were diluted to a volume of 100 µL prior to desalting. Desalting was performed
514 using 10mg Strata-X 33µm polymeric reversed phase SPE columns (Phenomenex, 8B-S100-AAK).
515 Each column was activated using 1 mL acetonitrile (ACN) (Honeywell, LC015) followed by of 1 mL
516 0.1% formic acid, 1 mL 0.1% formic acid in 50% ACN, and equilibration with addition of 1 mL 0.1%
517 formic acid. After equilibration, the samples were added to the column and rinsed with 200 µL
518 0.1% formic acid. The columns were transferred to a 1.5 mL tube for elution by two additions of
519 150 µL 0.1% formic acid in 50% ACN. The eluent was then dried using a vacuum concentrator
520 (LabConco) prior to reconstitution in 10 µL of 0.1% formic acid.

521 Samples were analyzed by online nanoflow liquid chromatography-tandem mass
522 spectrometry using an Orbitrap Eclipse Tribrid mass spectrometer (Thermo Fisher Scientific)
523 coupled to a Dionex UltiMate 3000 HPLC (Thermo Fisher Scientific). For each analysis, 5µL was
524 injected onto an Acclaim PepMap 100 column packed with 2 cm of 5µm C18 material (Thermo
525 Fisher, 164564) using 0.1% formic acid in water (solvent A). Peptides were then separated on a

526 15cm PepMap RSLC EASY-Spray C18 Column packed with 2µm C18 material (Thermo Fisher,
527 ES904) using a gradient from 0-35% solvent B. (0.1% formic acid with 80% CAN) in 60 minutes.
528 Full scan MS1 spectra were collected at a resolution of 60,000, an automatic gain control of 1E5,
529 and a mass range from 400-1500 m/z. Dynamic exclusion was enabled with a repeat count of 2
530 and repeat and duration of 8 seconds. Only charge states 2 to 6 were selected for fragmentation.
531 MS2s were generated at top speed for 3 seconds. Higher-energy collisional dissociation (HCD)
532 was performed on all selected precursor masses with the following parameters: isolation window
533 of 2m/z, stepped collision energies of 25%, 30%, 40%, orbitrap detection (resolution of 7500),
534 maximum inject time of 75ms, and a standard AGC target.

535 Label-free quantification was performed using the minimal workflow for MaxQuant
536 according to the established protocol for standard data sets.[79] Files were searched with fully
537 specific cleavage C-terminal to an Arg or Lys residue, with 2 allowed missed cleavages.
538 Carbamidomethyl Cys was set as a fixed modification. Raw data generated from each intestinal
539 section was included and analyzed using Perseus, according to the recommended protocol for
540 label-free interaction data (Fold change >5 as the cutoff).

541 ***Fecal DNA Extraction and 16S rRNA Gene Sequencing:*** DNA was isolated from fecal
542 pellets using the phenol/chloroform method as described.[7] Samples were then processed with
543 QIAquick PCR purification kit (Qiagen #28106). Full protocol is outlined below:

544 250µL of 0.1 mm zirconia/silica beads (BioSpec #11079101z) were added to a sterile 2 mL
545 screwtop tube (Celltreat #230830). One 4 mm steel ball was added to each tube (BioSpec
546 #11079132ss). 500µL of Buffer A (200 mM TrisHCl, pH 8.0, 200 mM NaCl, 20 mM EDTA) and 210µL

547 of 20% SDS were added to each fecal pellet in a separate 1.7mL tube. Pellets were vortexed and
548 supernatant transferred to the 2mL screwtop tube containing beads. 500µL of
549 Phenol/chloroform/IAA were added to each screwtop tube. Tubes were allowed to beadbeat on
550 high for 4 min at room temperature. Samples were then centrifuge at 12000 rpm for 5 min at
551 4°C. 420µL of the aqueous layer were transferred to a new 1.7mL tube. 100uL of samples were
552 then processed using the Qiagen PCR Purification Kit

553 ***3 week UCMRS experiments:*** The V4 region of the 16S rRNA gene was amplified from
554 each sample using a dual indexing sequencing strategy.[80] Samples were sequenced on the MiSeq
555 platform (Illumina) using the MiSeq Reagent Kit v2 (500 cycles, Illumina #MS102-2003) according
556 to the manufacturer's protocol with modifications found in the Schloss Wet Lab SOP
557 (https://github.com/SchlossLab/MiSeq_WetLab_SOP).
558

559 ***Fig 1 16S Sequence Analysis:*** All processing and analysis of 16S rRNA sequencing data was
560 performed in R (version 4.1.2).[81] Raw sequencing reads were processed for downstream analysis
561 using DADA2 (version 1.22.0).[82] Processing included inspection of raw reads for quality, filtering
562 of low-quality reads, merging of paired reads, and removal of chimeric sequences. Length
563 distribution of non-chimeric sequences was plotted to ensure lengths matched the expected V4
564 amplicon size. Taxonomy was assigned to amplicon sequence variants (ASVs) by aligning reads
565 with the Silva reference database (version 138.1).[83]
566 Microbiota diversity and community composition were analyzed using the packages
567 phyloseq (version 1.38.0), microbiome (version 1.16.0), and vegan (version 2.5.7).[84-86] The
568 packages tidyverse (version 1.3.0), and ggplot2 (version 3.3.5) were used for data organization

569 and visualization.[87,88] Random forest analysis was performed using the and randomForest
570 (version 4.6.14), vegan (version 6.0.90), and pROC (version 1.18.0) packages.[89-91]
571 Samples were first divided into training (70% of samples, divided equally between
572 Baseline and Stressed samples) and test (30% of samples) sets. The training set was used to tune
573 the "mtry" parameter of the model, while the test set was used to validate model performance.
574 Feature importance was determined using the Gini index, which measures the total decrease in
575 node impurity averaged across all trees.
576 Custom code and detailed instructions can be found at:
577 https://github.com/gbmoreau/Gautier-manuscript. Raw sequencing reads can be found in the
578 NCBI Sequence Read Archive (SRA) database under PRJNA867333.
579
580 ***Microbiome Transfer Experiments:*** Antibiotic microbiome transfer experiments were
581 performed by treating mice with a cocktail of the following antibiotics: Ampicillin (Sigma-Aldrich,
582 A8351), Neomycin (Sigma-Aldrich, N6386), Metronidazole (Sigma-Aldrich, M1547), and
583 Vancomycin (Sigma-Aldrich, V1130). Ampicillin, Neomycin, and Metronidazole were added to
584 water containing 8g/L of a zero-calorie sweetener at 1g/L. Vancomycin was added at 500mg/L.
585 Mice were allowed to drink ad labium for two weeks and fresh antibiotic solutions were made
586 once per week. After 2 weeks of antibiotic treatment, mice were given an oral gavage of 100uL
587 of either naïve or stressed fecal slurry (equal weights of collected fecal pellets homogenized in
588 4mL PBS) every 2 days for a total of 4 gavage treatments. Animals were allowed to habituate to
589 the introduced microbiome for 14 days from the first gavage. Germ free experiments were
590 performed as described.[39]

591

592 ***Microbiome Transfer and 1 week UCMRS 16S**:* Fecal pellet DNA extraction and 16S
593 sequencing of the V4 region was performed by Zymo according to their protocols. Raw
594 sequencing reads can be found in the NCBI Sequence Read Archive (SRA) database under
595 PRJNA878703 and PRJNA866924, respectively.

596

597 ***Cell Culture:*** HT-29 cells were purchased from ATCC and were grown in McCoy's 5A media
598 (ATCC 30-2007) as per the ATCC website. Cells were plated at a density of 150,000/well and
599 allowed to adhere to 12 well plates overnight in complete media. Cells were treated with 10μM
600 of either NTC (Sigma-Aldrich, SMB00208) or BI6015 (Sigma-Aldrich, 375240) for 24hrs. After 24
601 hours, media was aspirated, and cells were frozen at -80 until RNA extraction was performed.

602

603 ***RNA and ChIP Seq Experiments:*** All ChIP Seq experiments were performed previously on
604 duodenal villus tissue as described.[48,49] Raw data can be found under GEO accession numbers
605 GSE112946 (RNA-seq and ChIP-seq) and GSE148691 (HiChIP-seq).

606

607 ***DeepLabCut:*** Deeplabcut analysis was performed as previously described.[62] Full protocol
608 is outlined below:

609 Animal pose estimation was performed by using a deep-learning package called
610 DeepLabCut. The detailed mathematical model and network architecture for DeepLabCut was
611 previously published by the Mathis lab [63]. We generated a DeepLabCut convolutional neural
612 network to analyze our open field test videos, which is trained in a supervised manner: 16

613 manually labeled points were selected as references of transfer learning, including nose, left and
614 right eyes, left and right ears, neck, left and right arm, left and right leg, 3 points on body and 3
615 points on tail. In total, 15 randomly selected videos were used for building a training dataset.
616 Finally, the performance of the neural network is evaluated by human researchers.

617 Estimated mouse poses from DeepLabCut were further analyzed by using a package called
618 Variational Animal Motion Embedding (VAME), which classifies animal behavior in an
619 unsupervised manner. VAME was developed by the Pavol Bauer group and the package can be
620 downloaded at https://github.com/LINCellularNeuroscience/VAME[92]. We trained a unique
621 VAME recursive neural network for each experiment, which classifies each frame of the open
622 field test video into 1 of the 25 behavioral motifs. Then, all behavior motifs were annotated and
623 evaluated by blinded human researchers. With annotated frames, we were able to calculate the
624 percentage of time usage of each motif, which is then used for principal component analysis and
625 Kullback-Leibler divergence analysis. Custom code is available upon request.

626 ***RNA Extraction and Quantitative PCR:*** For RNA extraction, cultured cells were pelleted,
627 frozen, and lysed. RNA was extracted using the Bioline Isolate II RNA mini kit as per manufacture's
628 protocol (BIO- 52073). RNA was quantified with a Biotek Epoch Microplate Spectrophotometer.
629 Normalized RNA was reverse transcribed to cDNA with either the Bioline SensiFast cDNA
630 Synthesis Kit (BIO-65054) or Applied Sciences High- Capacity cDNA Reverse Transcriptase Kit (43-
631 688-13). cDNA was amplified using the Bioline SensiFast NO- ROX kit (BIO-86020), according to
632 manufacturer's instructions. Results were analyzed with the relative quantity (ΔΔCq) method.
633 Probes used are listed in Extended Data 5, Tab 4.

634 ***Immunofluorescence Staining and Imaging:*** 1cm sections of intestinal samples were
635 harvested and snap frozen in an OCT block (Fisher Scientific #14-373-65). Samples were cut on a
636 cryostat in 15μM sections and placed on microscope slides. Tissue was fixed directly on the slides
637 in carnoy's solution (60% Ethanol, 30% Chloroform, and 10% Glacial Acetic Acid) for 10 min at
638 room temperature. Tissue was washed in 1x PBS for 5 min 3x at room temperature. Antigen
639 retrieval was performed with Tris-EDTA by bringing solution to a boil (~30sec) in a microwave.
640 Slides were washed in 1x PBS 3x for 5 min at room temperature. After final wash, sections were
641 outlined with a hydrophobic pen (Vector Laboratories #H-4000). Samples were blocked for 1 hour
642 at room temperature with 1:200 FC block in TBST (1x TBS + 0.3% Triton X-100) plus 2% Normal
643 Donkey Serum (Jackson ImmunoResearch #017-000-121). Supernatant was removed and
644 samples were blocked with Mouse on Mouse IgG for 1 hour at room temperature (Vector
645 Laboratories #MKB-2213-1) plus 2% Normal Donkey Serum. Supernatant was removed and
646 primary antibodies were added. Samples were stained with 1:1000 Mucin 13 (G-10) (Santa Cruz
647 Biotechnology #sc-390115) and 1:1000 Mucin 2 (GeneTex #GTX100664) overnight at 4 degrees
648 Celsius in blocking solution (1x PBS, 0.5g bovine serum albumin, 0.5% Triton X-100) + 2% normal
649 donkey serum. Control samples were stained in blocking solution + 2% normal donkey serum
650 with mouse IgG (Jackson ImmunoResearch #015-000-003) or rabbit IgG (Jackson
651 ImmunoResearch #011-000-003) diluted to match the primary antibodies. The next day samples
652 were washed in TBST for 5 min 3x at room temperature. Samples were then incubated in
653 secondary antibodies for 3 hours at room temperature in blocking solution + 2% normal donkey
654 serum. Secondary antibodies used were Donkey Anti-Mouse 488 (Jackson ImmunoResearch
655 #715-545-150) and Donkey Anti-Rabbit 647 (Jackson ImmunoResearch #711-605-152).

656 Secondaries were added at 2mg/mL. Samples were then stained with Hoechst (1:700) (Thermo
657 Fisher Scientific #H3570) for 15 min in blocking solution + 2% normal donkey serum. Samples
658 were washed 2x with TBST for 5 min at room temperature. Samples were washed a final time in
659 TBS for 5 min at room temperature. Finally, slides imaged on a Leica Stellaris 5 confocal
660 microscope.

661

662 **QUANTIFICATION AND STATISTICAL ANALYSIS**

663 ***Statistical analysis:*** All statistical analyses-except those associated with DeepLabCut,
664 Mass Spectrometry, and 16S were performed in GraphPad Prism 9. Analyses comparing two
665 groups were performed using a two-tailed T test. If the variances between groups were
666 significantly different, a Welch's correction was applied. Outliers were excluded if they fell more
667 than two standard deviations from the mean. For all analyses, the threshold for significance was
668 at $p < 0.05$. Repeats for each experiment are specified in the figure legend corresponding to the
669 respective panel. Additional statistical detail, including all p-values, can be found in Ext. Data 5,
670 Tab 5.

671

672 **Acknowledgements:** The mass spectrometry experiments in Figure 1 were performed in the UVA
673 Biomolecular Research Facility Core. The W.M. Keck Biomedical Mass Spectrometry Laboratory
674 is funded by a grant from the University of Virginia's School of Medicine. Alexandria Battison
675 provided additional technical assistance in Mass Spectrometry experiments.

676

677 **Contributions:** C.R.N. and A.G. designed the study; C.R.N., A.R.M., C.R., N.M.G., R.M.B., R.B., A.K.,
678 R.O., A.D.S., K.E.M., S.A.M., M.V, and C.D. performed and conceptualized experiments; G.B.M.,
679 S.L., D.E.O, T.M.H.P., K.V., L.C., and J.B.S. performed sequencing and DeepLabCut analysis; C.R.N
680 and A.G. analyzed and wrote the manuscript; A.G. oversaw the project.

681 **Competing Interests:** S.A.M. is an inventor on a Stanford patent related to the use of mucinases
682 as research tools; she is also a consultant for InterVenn Biosciences.

683 **Funding:** The authors are supported by grants from the UVA Trans University Microbiome
684 Initiative pilot grant, Cat Miller Foundation, and the Owens Family Foundation. C.R.N is supported
685 by the UVA Presidential Fellowship in Neuroscience. A.R.M. is supported by the NINDS T32
686 NS115657 and F31 AI174782. Work from the R.O., K.V., and L.C. from the lab of M.V. was
687 supported by NIH grants R01DK121915 and R01DK126446. A.D.S. is supported by the National
688 Institutes of Health Chemical Biology Training Grant (T32 GM067543). K.E.M. is supported by the
689 Yale Endowed Postdoctoral Fellowship in the Biological Sciences.

690

691

692

693

694

695 **References:**

696 1 Santomauro, D. F. *et al.* Global prevalence and burden of depressive and anxiety
697 disorders in 204 countries and territories in 2020 due to the COVID-19 pandemic. *The*
698 *Lancet* **398**, 1700-1712, doi:https://doi.org/10.1016/S0140-6736(21)02143-7 (2021).

2 Fava, M. Diagnosis and definition of treatment-resistant depression. *Biological Psychiatry* **53**, 649-659, doi:https://doi.org/10.1016/S0006-3223(03)00231-2 (2003).

3 Heim, C. & Binder, E. B. Current research trends in early life stress and depression: Review of human studies on sensitive periods, gene–environment interactions, and epigenetics. *Experimental Neurology* **233**, 102-111, doi:https://doi.org/10.1016/j.expneurol.2011.10.032 (2012).

4 McGonagle, K. A. & Kessler, R. C. Chronic stress, acute stress, and depressive symptoms. *American Journal of Community Psychology* **18**, 681-706, doi:https://doi.org/10.1007/BF00931237 (1990).

5 Lach, G., Schellekens, H., Dinan, T. G. & Cryan, J. F. Anxiety, Depression, and the Microbiome: A Role for Gut Peptides. *Neurotherapeutics : the journal of the American Society for Experimental NeuroTherapeutics* **15**, 36-59, doi:10.1007/s13311-017-0585-0 (2018).

6 Foster, J. A. & McVey Neufeld, K. A. Gut-brain axis: how the microbiome influences anxiety and depression. *Trends in neurosciences* **36**, 305-312, doi:10.1016/j.tins.2013.01.005 (2013).

7 Marin, I. A. *et al.* Microbiota alteration is associated with the development of stress-induced despair behavior. *Scientific reports* **7**, 43859-43859, doi:10.1038/srep43859 (2017).

8 Tian, P. *et al.* Bifidobacterium breve CCFM1025 attenuates major depression disorder via regulating gut microbiome and tryptophan metabolism: A randomized clinical trial. *Brain, behavior, and immunity* **100**, 233-241, doi:https://doi.org/10.1016/j.bbi.2021.11.023 (2022).

9 Berding, K. & Cryan, J. F. Microbiota-targeted interventions for mental health. *Curr Opin Psychiatry* **35**, 3-9, doi:10.1097/yco.0000000000000758 (2022).

10 Valles-Colomer, M. *et al.* The neuroactive potential of the human gut microbiota in quality of life and depression. *Nature Microbiology* **4**, 623-632, doi:10.1038/s41564-018-0337-x (2019).

11 Park, S.-Y. *et al.* Strain-level fitness in the gut microbiome is an emergent property of glycans and a single metabolite. *Cell* **185**, 513-529.e521, doi:10.1016/j.cell.2022.01.002 (2022).

12 Zmora, N. *et al.* Personalized Gut Mucosal Colonization Resistance to Empiric Probiotics Is Associated with Unique Host and Microbiome Features. *Cell* **174**, 1388-1405.e1321, doi:https://doi.org/10.1016/j.cell.2018.08.041 (2018).

13 Borisova, M. A. *et al.* Mucin-2 knockout is a model of intercellular junction defects, mitochondrial damage and ATP depletion in the intestinal epithelium. *Scientific reports* **10**, 21135, doi:10.1038/s41598-020-78141-4 (2020).

14 Hansson, G. C. Mucins and the Microbiome. *Annual Review of Biochemistry* **89**, 769-793, doi:10.1146/annurev-biochem-011520-105053 (2020).

15 Johansson, M. E. V. *et al.* Composition and functional role of the mucus layers in the intestine. *Cellular and Molecular Life Sciences* **68**, 3635, doi:10.1007/s00018-011-0822-3 (2011).

16 Van der Sluis, M. *et al.* Muc2-Deficient Mice Spontaneously Develop Colitis, Indicating That MUC2 Is Critical for Colonic Protection. *Gastroenterology* **131**, 117-129, doi:https://doi.org/10.1053/j.gastro.2006.04.020 (2006).

17 Velcich, A. *et al.* Colorectal cancer in mice genetically deficient in the mucin Muc2. *Science (New York, N.Y.)* **295**, 1726-1729, doi:10.1126/science.1069094 (2002).

18 Johansson, M. E. V. a. H., G. C. *The Mucins* Vol. 2 381-388 (2016).

19 Pelaseyed, T. & Hansson, G. C. Membrane mucins of the intestine at a glance. *Journal of Cell Science* **133**, jcs240929, doi:10.1242/jcs.240929 (2020).

20 Van Herreweghen, F., De Paepe, K., Marzorati, M. & Van de Wiele, T. Mucin as a Functional Niche is a More Important Driver of in Vitro Gut Microbiota Composition and Functionality than Supplementation of Akkermansia m uciniphila. *Applied and environmental microbiology* **87**, doi:10.1128/aem.02647-20 (2020).

21 Duncan, K., Carey-Ewend, K. & Vaishnava, S. Spatial analysis of gut microbiome reveals a distinct ecological niche associated with the mucus layer. *Gut Microbes*, 1-21, doi:10.1080/19490976.2021.1874815 (2021).

22 Sicard, J.-F., Le Bihan, G., Vogeleer, P., Jacques, M. & Harel, J. Interactions of Intestinal Bacteria with Components of the Intestinal Mucus. *Frontiers in cellular and infection microbiology* **7**, 387-387, doi:10.3389/fcimb.2017.00387 (2017).

23 Werlang, C., Cárcarmo-Oyarce, G. & Ribbeck, K. Engineering mucus to study and influence the microbiome. *Nature Reviews Materials* **4**, 134-145, doi:10.1038/s41578-018-0079-7 (2019).

24 Sommer, F. *et al.* Altered Mucus Glycosylation in Core 1 O-Glycan-Deficient Mice Affects Microbiota Composition and Intestinal Architecture. *PloS one* **9**, e85254, doi:10.1371/journal.pone.0085254 (2014).

25 Fu, J. *et al.* Loss of intestinal core 1-derived O-glycans causes spontaneous colitis in mice. *J Clin Invest* **121**, 1657-1666, doi:10.1172/jci45538 (2011).

26 Biol-N'garagba, M.-C., Niepceron, E., Mathian, B. & Louisot, P. Glucocorticoid-induced maturation of glycoprotein galactosylation and fucosylation processes in the rat small intestine. *The Journal of Steroid Biochemistry and Molecular Biology* **84**, 411-422, doi:https://doi.org/10.1016/S0960-0760(03)00062-1 (2003).

27 Silva, S. D. *et al.* Stress disrupts intestinal mucus barrier in rats via mucin O-glycosylation shift: prevention by a probiotic treatment. *American Journal of Physiology-Gastrointestinal and Liver Physiology* **307**, G420-G429, doi:10.1152/ajpgi.00290.2013 (2014).

28 Gong, S. *et al.* Dynamics and correlation of serum cortisol and corticosterone under different physiological or stressful conditions in mice. *PloS one* **10**, e0117503-e0117503, doi:10.1371/journal.pone.0117503 (2015).

29 Luo, Y. *et al.* Gut microbiota regulates mouse behaviors through glucocorticoid receptor pathway genes in the hippocampus. *Translational psychiatry* **8**, 187, doi:10.1038/s41398-018-0240-5 (2018).

30 Dodiya, H. B. *et al.* Chronic stress-induced gut dysfunction exacerbates Parkinson's disease phenotype and pathology in a rotenone-induced mouse model of Parkinson's disease. *Neurobiology of disease* **135**, 104352, doi:10.1016/j.nbd.2018.12.012 (2020).

31 Saldanha, D., Kumar, N., Ryali, V., Srivastava, K. & Pawar, A. A. Serum Serotonin Abnormality in Depression. *Medical Journal Armed Forces India* **65**, 108-112, doi:https://doi.org/10.1016/S0377-1237(09)80120-2 (2009).

32 Pfleiderer, B. *et al.* Effective electroconvulsive therapy reverses glutamate/glutamine deficit in the left anterior cingulum of unipolar depressed patients. *Psychiatry Research: Neuroimaging* **122**, 185-192, doi:https://doi.org/10.1016/S0925-4927(03)00003-9 (2003).

33 Bailey, M. T. *et al.* Exposure to a social stressor alters the structure of the intestinal microbiota: implications for stressor-induced immunomodulation. *Brain, behavior, and immunity* **25**, 397-407, doi:10.1016/j.bbi.2010.10.023 (2011).

34 Bastiaanssen, T. F. S. *et al.* Gutted! Unraveling the Role of the Microbiome in Major Depressive Disorder. *Harv Rev Psychiatry* **28**, 26-39, doi:10.1097/HRP.0000000000000243 (2020).

35 Li, N. *et al.* Fecal microbiota transplantation from chronic unpredictable mild stress mice donors affects anxiety-like and depression-like behavior in recipient mice via the gut microbiota-inflammation-brain axis. *Stress* **22**, 592-602, doi:10.1080/10253890.2019.1617267 (2019).

36 Karl, J. P. *et al.* Changes in intestinal microbiota composition and metabolism coincide with increased intestinal permeability in young adults under prolonged physiological stress. *American journal of physiology. Gastrointestinal and liver physiology* **312**, G559-g571, doi:10.1152/ajpgi.00066.2017 (2017).

37 Hansson, G. C. Mucins and the Microbiome. *Annu Rev Biochem*, doi:10.1146/annurev-biochem-011520-105053 (2020).

38 Sicard, J. F., Le Bihan, G., Vogeleer, P., Jacques, M. & Harel, J. Interactions of Intestinal Bacteria with Components of the Intestinal Mucus. *Frontiers in cellular and infection microbiology* **7**, 387, doi:10.3389/fcimb.2017.00387 (2017).

39 Merchak, A. R. *et al.* Lactobacillus maintains IFNγ homeostasis to promote behavioral stress resilience. *bioRxiv*, 2023.2005.2010.540223, doi:10.1101/2023.05.10.540223 (2023).

40 Johansson, M. E. *et al.* Normalization of Host Intestinal Mucus Layers Requires Long-Term Microbial Colonization. *Cell Host Microbe* **18**, 582-592, doi:10.1016/j.chom.2015.10.007 (2015).

41 Kent, W. J. *et al.* The human genome browser at UCSC. *Genome Res* **12**, 996-1006, doi:10.1101/gr.229102 (2002).

42 Chahar, S. *et al.* Chromatin profiling reveals regulatory network shifts and a protective role for hepatocyte nuclear factor 4α during colitis. *Mol Cell Biol* **34**, 3291-3304, doi:10.1128/mcb.00349-14 (2014).

43 Lickwar, C. R. *et al.* Transcriptional Integration of Distinct Microbial and Nutritional Signals by the Small Intestinal Epithelium. *Cellular and molecular gastroenterology and hepatology* **14**, 465-493, doi:https://doi.org/10.1016/j.jcmgh.2022.04.013 (2022).

44 Babeu, J. P. & Boudreau, F. Hepatocyte nuclear factor 4-alpha involvement in liver and intestinal inflammatory networks. *World journal of gastroenterology* **20**, 22-30, doi:10.3748/wjg.v20.i1.22 (2014).

45 Chen, L. *et al.* The nuclear receptor HNF4 drives a brush border gene program conserved across murine intestine, kidney, and embryonic yolk sac. *Nature Communications* **12**, 2886, doi:10.1038/s41467-021-22761-5 (2021).
46 Shurer, C. R. *et al.* Physical Principles of Membrane Shape Regulation by the Glycocalyx. *Cell* **177**, 1757-1770.e1721, doi:https://doi.org/10.1016/j.cell.2019.04.017 (2019).
47 Lu, H. *et al.* Crosstalk of hepatocyte nuclear factor 4a and glucocorticoid receptor in the regulation of lipid metabolism in mice fed a high-fat-high-sugar diet. *Lipids in Health and Disease* **21**, 46, doi:10.1186/s12944-022-01654-6 (2022).
48 Chen, L. *et al.* A reinforcing HNF4-SMAD4 feed-forward module stabilizes enterocyte identity. *Nat Genet* **51**, 777-785, doi:10.1038/s41588-019-0384-0 (2019).
49 Chen, L. *et al.* Three-dimensional interactions between enhancers and promoters during intestinal differentiation depend upon HNF4. *Cell reports* **34**, doi:10.1016/j.celrep.2020.108679 (2021).
50 Chen, L. *et al.* HNF4 Regulates Fatty Acid Oxidation and Is Required for Renewal of Intestinal Stem Cells in Mice. *Gastroenterology* **158**, 985-999.e989, doi:10.1053/j.gastro.2019.11.031 (2020).
51 Gupta, B. K. *et al.* Functions and regulation of MUC13 mucin in colon cancer cells. *J Gastroenterol* **49**, 1378-1391, doi:10.1007/s00535-013-0885-z (2014).
52 Darsigny, M. *et al.* Hepatocyte Nuclear Factor-4α Promotes Gut Neoplasia in Mice and Protects against the Production of Reactive Oxygen Species. *Cancer research* **70**, 9423-9433, doi:10.1158/0008-5472.Can-10-1697 (2010).
53 Kiselyuk, A. *et al.* HNF4α antagonists discovered by a high-throughput screen for modulators of the human insulin promoter. *Chem Biol* **19**, 806-818, doi:10.1016/j.chembiol.2012.05.014 (2012).
54 Lee, S. H., Veeriah, V. & Levine, F. A potent HNF4α agonist reveals that HNF4α controls genes important in inflammatory bowel disease and Paneth cells. *PloS one* **17**, e0266066, doi:10.1371/journal.pone.0266066 (2022).
55 Gurumurthy, C. B. *et al.* Creation of CRISPR-based germline-genome-engineered mice without ex vivo handling of zygotes by i-GONAD. *Nature Protocols* **14**, 2452-2482, doi:10.1038/s41596-019-0187-x (2019).
56 Ohtsuka, M. *et al.* i-GONAD: a robust method for in situ germline genome engineering using CRISPR nucleases. *Genome Biology* **19**, 25, doi:10.1186/s13059-018-1400-x (2018).
57 Malaker, S. A. *et al.* The mucin-selective protease StcE enables molecular and functional analysis of human cancer-associated mucins. *Proceedings of the National Academy of Sciences* **116**, 7278-7287, doi:10.1073/pnas.1813020116 (2019).
58 Malaker, S. A. *et al.* Revealing the human mucinome. *Nature Communications* **13**, 3542, doi:10.1038/s41467-022-31062-4 (2022).
59 Pothion, S., Bizot, J.-C., Trovero, F. & Belzung, C. Strain differences in sucrose preference and in the consequences of unpredictable chronic mild stress. *Behavioural brain research* **155**, 135-146, doi:https://doi.org/10.1016/j.bbr.2004.04.008 (2004).
60 Peng, Y.-L. *et al.* Inducible nitric oxide synthase is involved in the modulation of depressive behaviors induced by unpredictable chronic mild stress. *Journal of neuroinflammation* **9**, 75, doi:10.1186/1742-2094-9-75 (2012).

61 Nollet, M., Guisquet, A.-M. L. & Belzung, C. Models of Depression: Unpredictable Chronic Mild Stress in Mice. *Current protocols in pharmacology* **61**, 5.65.61-65.65.17, doi:https://doi.org/10.1002/0471141755.ph0565s61 (2013).
62 Rivet-Noor, C. R. *et al.* Stress-induced despair behavior develops independently of the Ahr-RORγt axis in CD4 + cells. *Scientific reports* **12**, 8594, doi:10.1038/s41598-022-12464-2 (2022).
63 Mathis, A. *et al.* DeepLabCut: markerless pose estimation of user-defined body parts with deep learning. *Nature Neuroscience* **21**, 1281-1289, doi:10.1038/s41593-018-0209-y (2018).
64 Bergstrom, K. *et al.* Proximal colon–derived O-glycosylated mucus encapsulates and modulates the microbiota. *Science (New York, N.Y.)* **370**, 467-472, doi:10.1126/science.aay7367 (2020).
65 Wu, M. *et al.* The Dynamic Changes of Gut Microbiota in Muc2 Deficient Mice. *International journal of molecular sciences* **19**, doi:10.3390/ijms19092809 (2018).
66 Bergstrom, K. S. *et al.* Muc2 protects against lethal infectious colitis by disassociating pathogenic and commensal bacteria from the colonic mucosa. *PLoS pathogens* **6**, e1000902, doi:10.1371/journal.ppat.1000902 (2010).
67 Johansson, M. E., Thomsson, K. A. & Hansson, G. C. Proteomic analyses of the two mucus layers of the colon barrier reveal that their main component, the Muc2 mucin, is strongly bound to the Fcgbp protein. *J Proteome Res* **8**, 3549-3557, doi:10.1021/pr9002504 (2009).
68 Johansson, M. E. V. *et al.* The inner of the two Muc2 mucin-dependent mucus layers in colon is devoid of bacteria. *Proceedings of the National Academy of Sciences* **105**, 15064-15069, doi:10.1073/pnas.0803124105 (2008).
69 Marczynski, M. *et al.* Structural Alterations of Mucins Are Associated with Losses in Functionality. *Biomacromolecules*, doi:10.1021/acs.biomac.1c00073 (2021).
70 Ware, E. B. *et al.* Comparative genome-wide association studies of a depressive symptom phenotype in a repeated measures setting by race/ethnicity in the multi-ethnic study of atherosclerosis. *BMC Genetics* **16**, 118, doi:10.1186/s12863-015-0274-0 (2015).
71 Dunn, E. C. *et al.* Genome-wide association study of depressive symptoms in the Hispanic Community Health Study/Study of Latinos. *Journal of psychiatric research* **99**, 167-176, doi:10.1016/j.jpsychires.2017.12.010 (2018).
72 Rivet-Noor, C. & Gaultier, A. The Role of Gut Mucins in the Etiology of Depression. *Front Behav Neurosci* **14**, 592388, doi:10.3389/fnbeh.2020.592388 (2020).
73 McClain, L. L. *et al.* Rare variants and biological pathways identified in treatment-refractory depression. *J Neurosci Res* **98**, 1322-1334, doi:10.1002/jnr.24609 (2020).
74 Vető, B. *et al.* The transcriptional activity of hepatocyte nuclear factor 4 alpha is inhibited via phosphorylation by ERK1/2. *PloS one* **12**, e0172020, doi:10.1371/journal.pone.0172020 (2017).
75 Gourley, S. L., Wu, F. J. & Taylor, J. R. Corticosterone Regulates pERK1/2 Map Kinase in a Chronic Depression Model. *Annals of the New York Academy of Sciences* **1148**, 509-514, doi:https://doi.org/10.1196/annals.1410.076 (2008).

76 Yang, C.-H., Huang, C.-C. & Hsu, K.-S. Behavioral Stress Modifies Hippocampal Synaptic Plasticity through Corticosterone-Induced Sustained Extracellular Signal-Regulated Kinase/Mitogen-Activated Protein Kinase Activation. *The Journal of Neuroscience* **24**, 11029-11034, doi:10.1523/jneurosci.3968-04.2004 (2004).

77 Yu, J. *et al.* Involvement of ERK1/2 signalling and growth-related molecules' expression in response to heat stress-induced damage in rat jejunum and IEC-6 cells. *International Journal of Hyperthermia* **26**, 538-555, doi:10.3109/02656736.2010.481276 (2010).

78 Herath, M., Hosie, S., Bornstein, J. C., Franks, A. E. & Hill-Yardin, E. L. The Role of the Gastrointestinal Mucus System in Intestinal Homeostasis: Implications for Neurological Disorders. *Frontiers in cellular and infection microbiology* **10**, doi:10.3389/fcimb.2020.00248 (2020).

79 Tyanova, S., Temu, T. & Cox, J. The MaxQuant computational platform for mass spectrometry-based shotgun proteomics. *Nature Protocols* **11**, 2301-2319, doi:10.1038/nprot.2016.136 (2016).

80 Kozich, J. J., Westcott, S. L., Baxter, N. T., Highlander, S. K. & Schloss, P. D. Development of a dual-index sequencing strategy and curation pipeline for analyzing amplicon sequence data on the MiSeq Illumina sequencing platform. *Applied and environmental microbiology* **79**, 5112-5120, doi:10.1128/aem.01043-13 (2013).

81 Team, R. C. R: A language and environment for statistical computing. R Foundation for Statistical Computing. doi:https://www.R-project.org/. (2021).

82 Callahan, B. J. *et al.* DADA2: High-resolution sample inference from Illumina amplicon data. *Nat Methods* **13**, 581-583, doi:10.1038/nmeth.3869 (2016).

83 Quast, C. *et al.* The SILVA ribosomal RNA gene database project: improved data processing and web-based tools. *Nucleic Acids Res* **41**, D590-596, doi:10.1093/nar/gks1219 (2013).

84 Jari Oksanen, F. G. B., Michael Friendly, Roeland Kindt, Pierre Legendre, Dan McGlinn, Peter R. & Minchin, R. B. O. H., Gavin L. Simpson, Peter Solymos, M. Henry H. Stevens, Eduard Szoecs and Helene Wagner. vegan: Community Ecology Package. R package version 2.5-7. doi:https://CRAN.R-project.org/package=vegan (2020).

85 McMurdie, P. J. & Holmes, S. phyloseq: An R Package for Reproducible Interactive Analysis and Graphics of Microbiome Census Data. *PloS one* **8**, e61217, doi:10.1371/journal.pone.0061217 (2013).

86 Leo Lahti, F. G. M. E., Sudarshan Shetty, Tuomas Borman, Domenick J. Braccia, Ruizhu Huang, Hector Corrada Bravo. Microbiome R package. doi:http://microbiome.github.io.

87 Hadley Wickham, M. A., Jennifer Bryan, Winston Cheng, Lucy D'Agostino, Romain François, Garrett Grolemund, Alex Hayes, Lionel Henry, Max Kuhn, Thomas Lin Pedersen. Welcome to the Tidyverse. *Journal of Open Source Software* **4**, 1686, doi:https://doi.org/10.21105/joss.01686 (2019).

88 Wickham, H. *ggplot2: Elegant Graphics for Data Analysis.* . (Springer-Verlag 2016).

89 Robin, X. *et al.* pROC: an open-source package for R and S+ to analyze and compare ROC curves. *BMC Bioinformatics* **12**, 77, doi:10.1186/1471-2105-12-77 (2011).

90 Classification and regression by randomForest (R news 2, 2002).

91 Kuhn, M. caret: Classification and Regression Training. *R package version 6.0-90* (2021).

958 92 Luxem, K., Fuhrmann, F., Kürsch, J., Remy, S. & Bauer, P. Identifying Behavioral Structure
959 from Deep Variational Embeddings of Animal Motion. *bioRxiv*, 2020.2005.2014.095430,
960 doi:10.1101/2020.05.14.095430 (2020).
961 93 Concordet, J.-P. & Haeussler, M. CRISPOR: intuitive guide selection for CRISPR/Cas9
962 genome editing experiments and screens. *Nucleic Acids Research* **46**, W242-W245,
963 doi:10.1093/nar/gky354 (2018).
964

MAIN FIGURES:

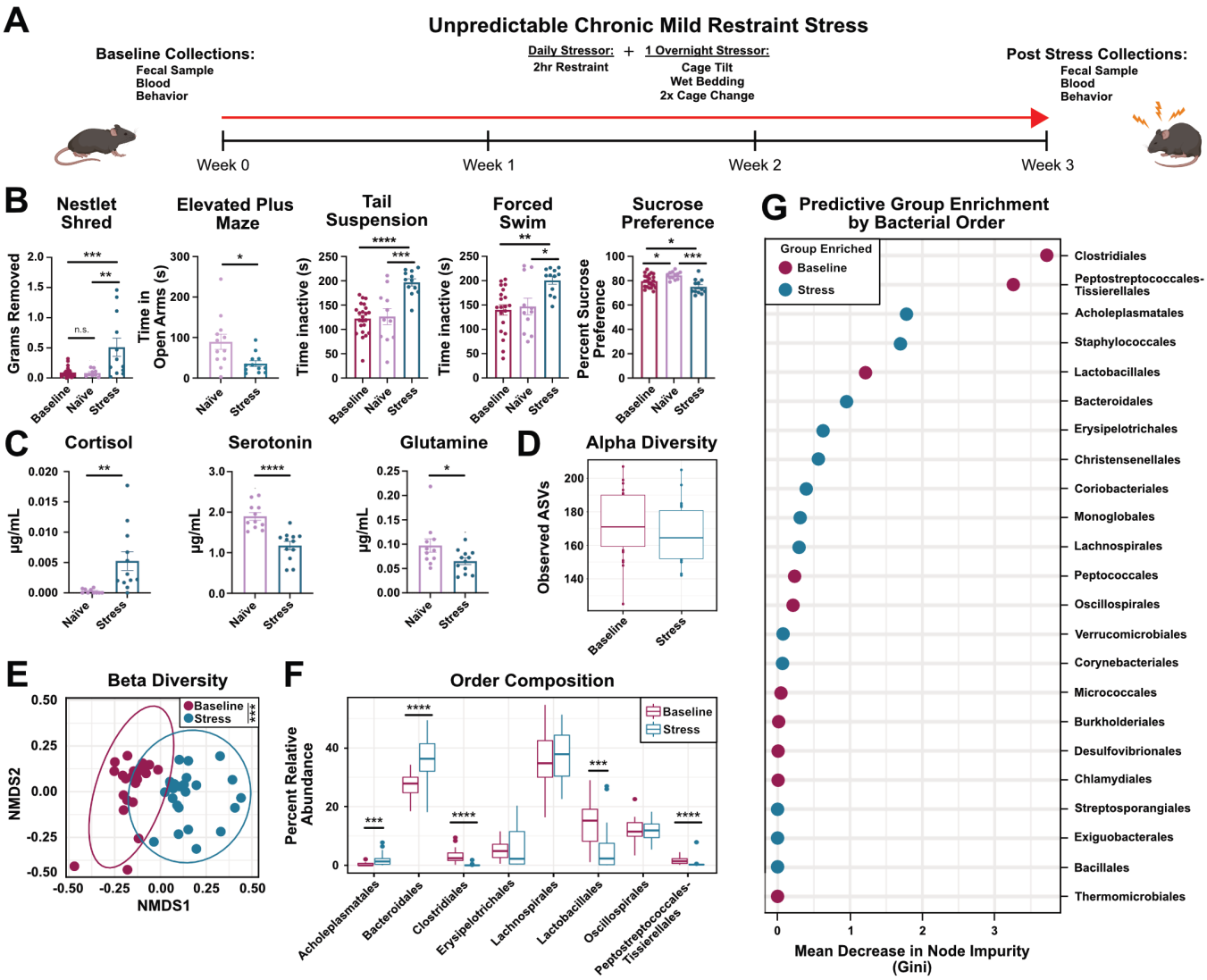

Figure 1: Unpredictable Chronic Mild Restraint Stress Induces Despair and Anxiety-Like Behaviors and Microbiome Dysbiosis: (A) Experimental Design. (B) Nestlet shred (One-way ANOVA), elevated plus maze (t-test), tail suspension (One-way ANOVA), forced swim (One-way ANOVA), and sucrose preference (One-way ANOVA) tests between baseline, naïve controls, and stress animals. Male mice, n=11/12 per group, representative of N=2. (C) Targeted mass

973 spectrometry from serum of naïve or stress animals (t-tests, n=11/12 per group). (D) Alpha
974 diversity plot showing microbial richness (observed ASVs) between baseline and stress mice
975 (Wilcoxon Rank Sum test). (E) NMDS plot of Bray-Curtis dissimilarity between baseline and stress
976 fecal microbiome samples (PERMANOVA). (F) Relative abundances of bacterial orders >1%
977 (Wilcoxon Rank Sum test with Bonferroni correction). (G) Importance plot from a random forest
978 model predicting bacterial orders that discriminate between baseline and stress groups.
979 Importance is based on the Gini index where larger values are more important to model. Male
980 mice, n=24/group, N=1.
981

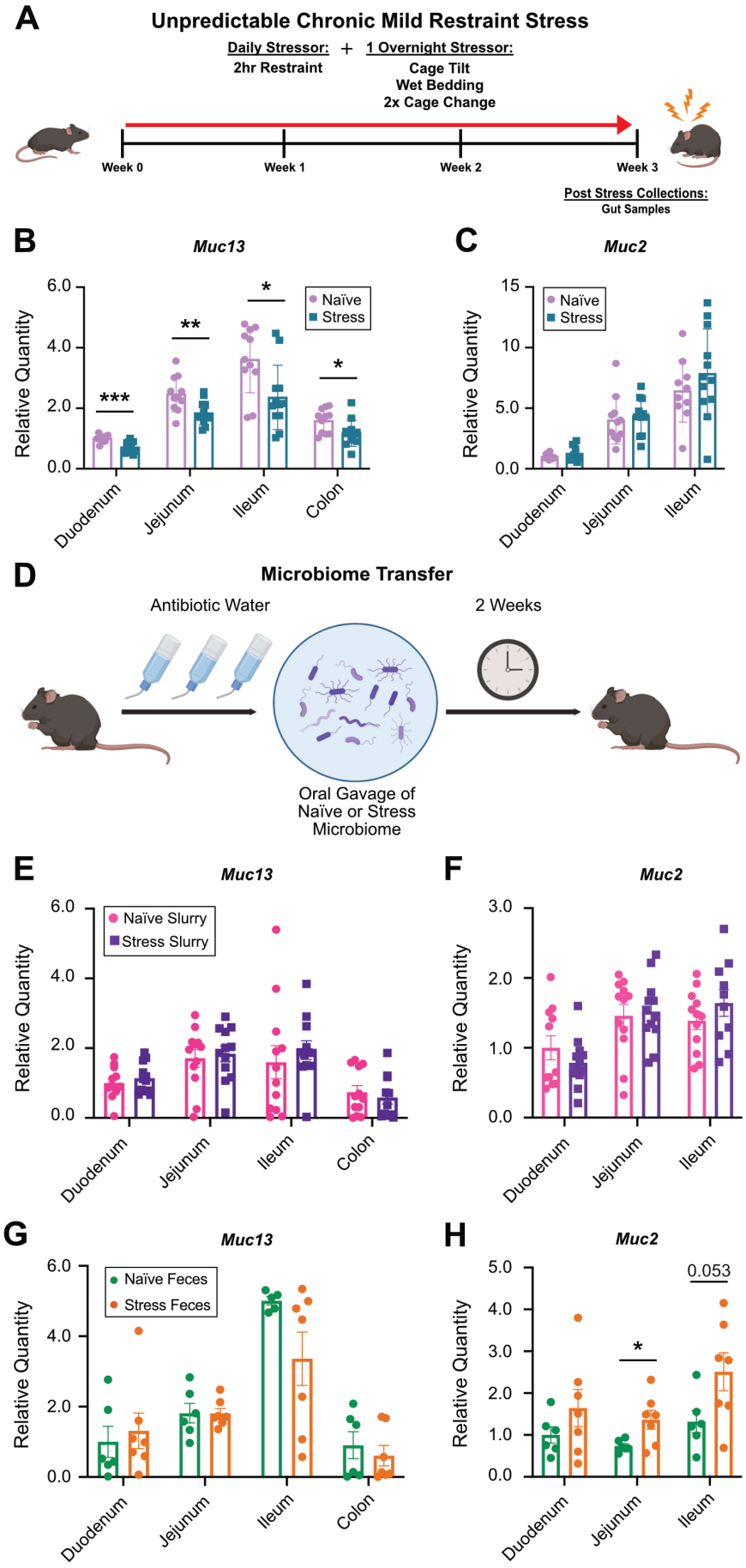
A
Unpredictable Chronic Mild Restraint Stress
Daily Stressor:
2hr Restraint
+
1 Overnight Stressor:
Cage Tilt
Wet Bedding
2x Cage Change
Week 0
Week 1
Week 2
Week 3
Post Stress Collections:
Gut Samples
B
Muc13
Naïve
Stress
Relative Quantity
Duodenum
Jejunum
Ileum
Colon
C
Muc2
D
Microbiome Transfer
Antibiotic Water
2 Weeks
Oral Gavage of
Naïve or Stress
Microbiome
E
Muc13
Naïve Slurry
Stress Slurry
F
Muc2
G
Muc13
Naïve Feces
Stress Feces
H
Muc2
0.053

982

983 **Figure 2: Stress Drives *Muc13* Reductions Independently of Transferrable Microbial Products:**
984 (A) Experimental design. Relative quantity of (B) *Muc13* and (C) *Muc2* transcripts by qPCR in
985 individual sections of the intestine. *Muc2* expression in the colon was higher than housekeeping
986 genes preventing quantification by qPCR. Unpaired two-tailed, t-tests. Male mice, n=11/12 per
987 group, N=2. (D) Experimental design. Relative quantity of (E) *Muc13* and (F) *Muc2* transcripts in
988 the intestines of animals receiving a naïve or stress fecal microbiome after antibiotic treatment
989 via gavage. Male mice, n=12 per group. T-tests, two-tailed. Relative quantity of (G) *Muc13* and
990 (H) *Muc2* in the intestines of germ-free mice given naïve or stress feces. Male mice, n=7 per
991 group. T-tests, two-tailed.
992

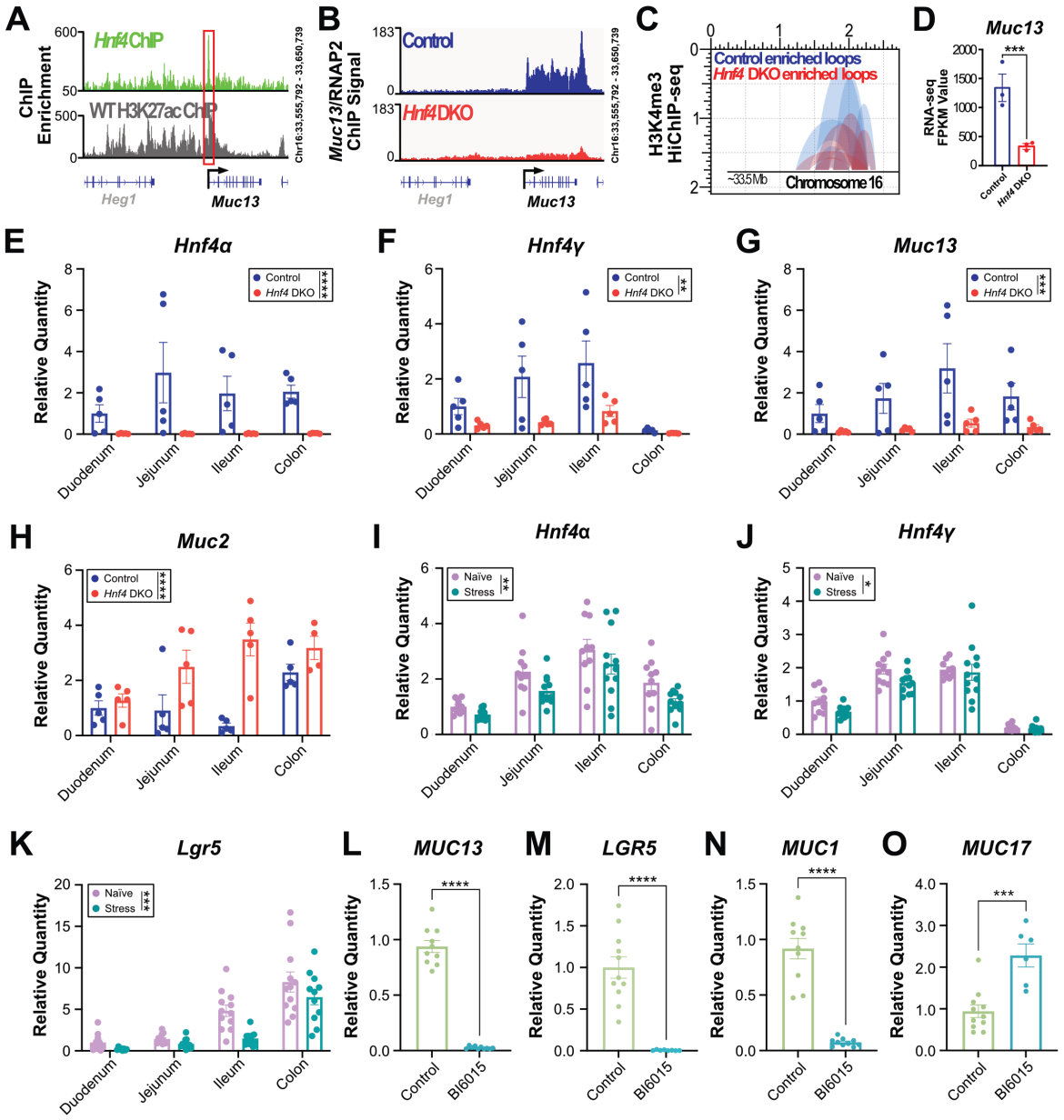

Figure 3: HNF4 Regulates Expression of *Muc13* both *In Vivo* and *In Vitro*: (A) HNF4 and H3K27ac ChIP-Seq of wildtype duodenal tissue at the *Muc13* promoter. (B) RNA Polymerase II ChIP-Seq in duodenal villus tissue in control and *Hnf4* DKO animals at the *Muc13* promoter. (C) H3K4me3 HiChIP-Seq examining chromatin loops in control and *Hnf4* DKO duodenal villus tissue at the *Muc13* promoter. (D) *Muc13* RNA-Seq fragments per kilobase per million in control and *Hnf4* DKO

duodenal tissue (stats performed with embedded cuffdiff package). All sequencing experiments performed on 3 mice/group. Relative quantity of (E) *Hnf4*α, (F) *Hnf4*γ, (G) *Muc13*, and (H) *Muc2* across the intestines in control and *Hnf4* DKO animals. Female mice, 5 mice/group. Two-way ANOVA. Relative quantities of (I) *Hnf4*α, (J) *Hnf4*γ, and (K) *Lgr5* across the intestines in naïve and stress animals. Male mice, 11-12 mice per group; Two-way ANOVA. Relative quantities of (L) *MUC13*, (M) *LGR5*, (N) *MUC1*, and (O) *MUC17* in human HT-29 cells treated for 24 hours with 10μM of HNF4 antagonist BI6015 or DMSO control. N=3, n=11. Two-tailed unpaired t-tests.

1007

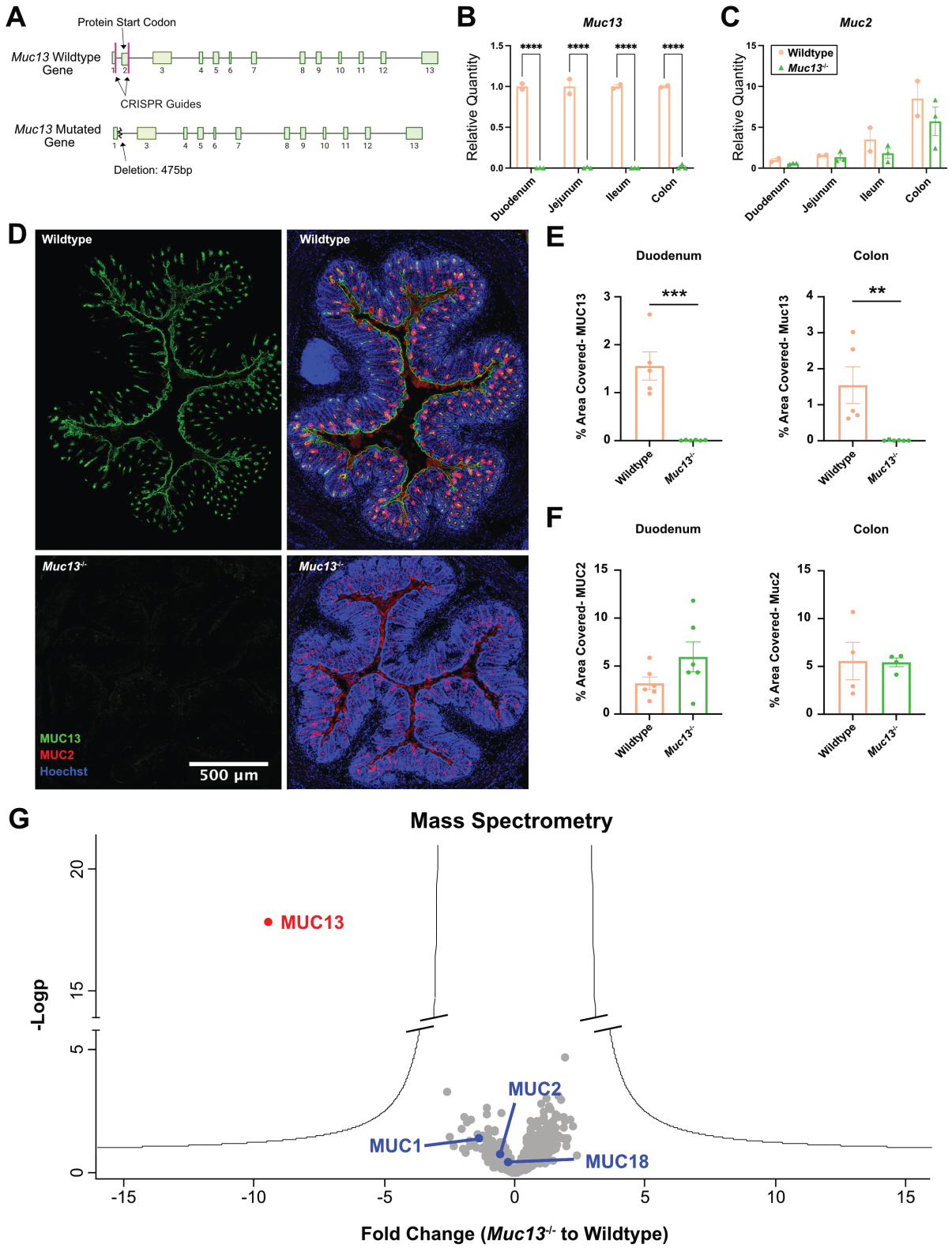
A
Protein Start Codon
Muc13 Wildtype Gene
CRISPR Guides
Muc13 Mutated Gene
Deletion: 475bp
B
Muc13
Relative Quantity
Duodenum
Jejunum
Ileum
Colon
C
Muc2
Wildtype
Muc13-/-
D
Wildtype
Muc13-/-
MUC13
MUC2
Hoechst
500 µm
E
Duodenum
Colon
% Area Covered- MUC13
% Area Covered- Muc13
F
% Area Covered- MUC2
% Area Covered- Muc2
G
Mass Spectrometry
-Logp
MUC13
MUC1
MUC2
MUC18
Fold Change (Muc13-/- to Wildtype)

1008

1009 **Figure 4: *Muc13* Deletion Validation:** (A) *Muc13* deletion schematic. Relative quantities of (B)
1010 *Muc13* and (C) *Muc2* in wildtype and *Muc13*$^{-/-}$ mice. Male mice, n=2-3 per group, N=1. T-tests,
1011 two-tailed. (D) Representative images of immunofluorescence (IF) staining of MUC13, MUC2 and
1012 Hoechst in the colon of wildtype and *Muc13*$^{-/-}$ animals. Quantification of IF of (E) MUC13 and (F)
1013 MUC2 in the duodenum and colon of wildtype and *Muc13*$^{-/-}$ mice. Male mice. T-tests, n=4-6 per
1014 group, N=2. (G) Fold change of mucins in the intestines of *Muc13*$^{-/-}$ compared to wildtype controls
1015 by mass spectrometry. All sections of the intestines are pooled for a total of 12 samples from 3
1016 mice per group. Male mice.
1017

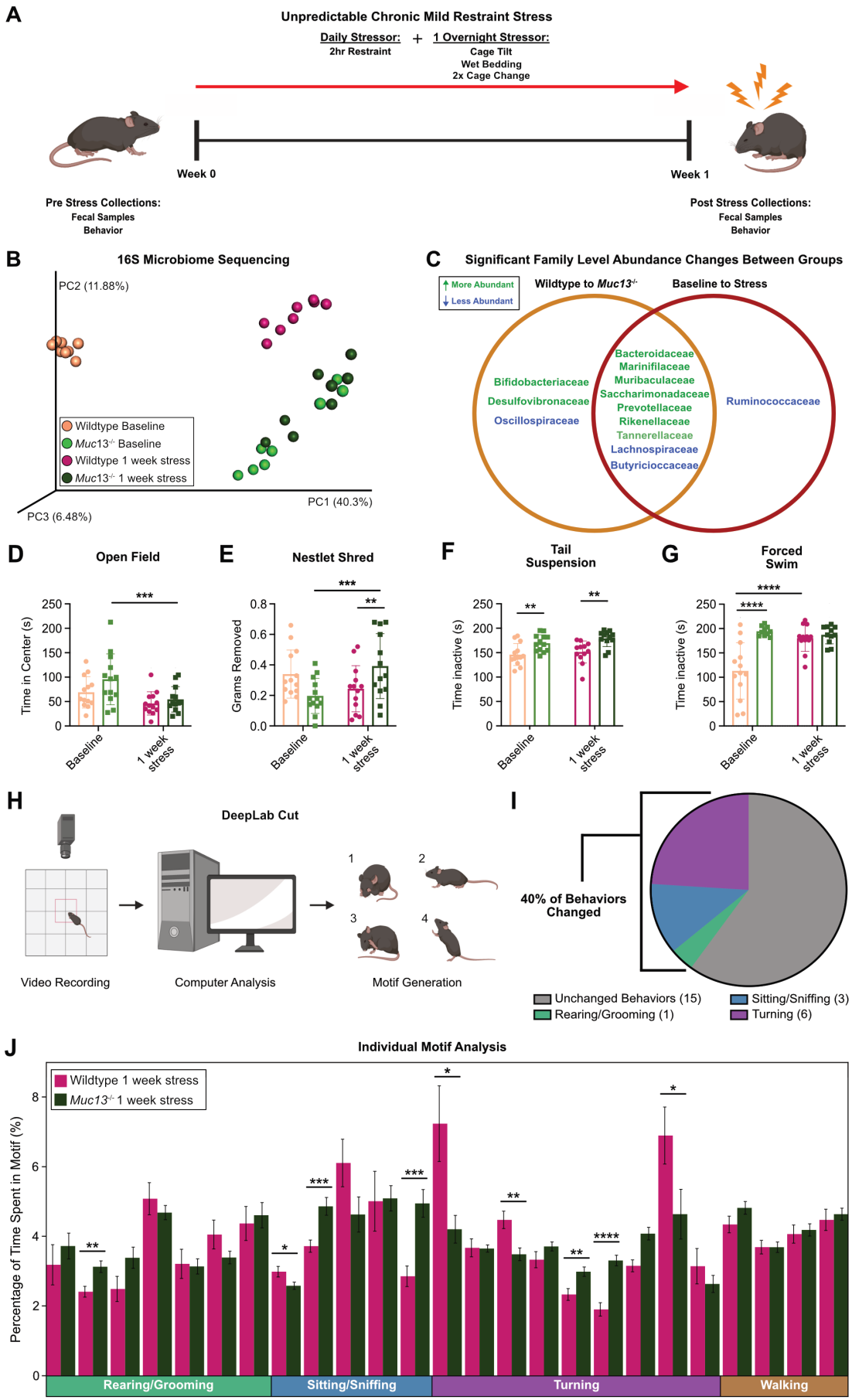
A
Unpredictable Chronic Mild Restraint Stress
Daily Stressor:
2hr Restraint
+
1 Overnight Stressor:
Cage Tilt
Wet Bedding
2x Cage Change
Week 0
Week 1
Pre Stress Collections:
Fecal Samples
Behavior
Post Stress Collections:
Fecal Samples
Behavior
B
16S Microbiome Sequencing
PC2 (11.88%)
PC1 (40.3%)
PC3 (6.48%)
Wildtype Baseline
Muc13-/- Baseline
Wildtype 1 week stress
Muc13-/- 1 week stress
C
Significant Family Level Abundance Changes Between Groups
More Abundant
Less Abundant
Wildtype to Muc13-/-
Baseline to Stress
Bifidobacteriaceae
Desulfovibronaceae
Oscillospiraceae
Bacteroidaceae
Marinifilaceae
Muribaculaceae
Saccharimonadaceae
Prevotellaceae
Rikenellaceae
Tannerellaceae
Lachnospiraceae
Butyricioccaceae
Ruminococcaceae
D
Open Field
Time in Center (s)
Baseline
1 week stress
E
Nestlet Shred
Grams Removed
F
Tail Suspension
Time inactive (s)
G
Forced Swim
H
DeepLab Cut
Video Recording
Computer Analysis
Motif Generation
I
40% of Behaviors Changed
Unchanged Behaviors (15)
Rearing/Grooming (1)
Sitting/Sniffing (3)
Turning (6)
J
Individual Motif Analysis
Wildtype 1 week stress
Muc13-/- 1 week stress
Percentage of Time Spent in Motif (%)
Rearing/Grooming
Sitting/Sniffing
Turning
Walking

1019 **Figure 5: Microbiome and Behavioral Changes in *Muc13*$^{-/-}$ Mice at Baseline and after Stress**
1020 **Exposure:** (A) Experimental design. (B) PCoA plot of 16S fecal microbial sequencing in wildtype
1021 and *Muc13*$^{-/-}$ animals at baseline and after 1 week of stress exposure. Male mice, n=8 per group,
1022 N=1. (C) Venn diagram comparing significantly changed families from 16S fecal microbiome
1023 sequencing between wildtype and *Muc13*$^{-/-}$ animals to families changes between wildtype
1024 baseline and stress exposed animals. (D) Open field and (E) nestlet shredding tests comparing
1025 anxiety-like behaviors between wildtype and *Muc13*$^{-/-}$ animals at baseline and after 1 week of
1026 stress exposure. (F) Tail suspension and (G) forced swim tests between wildtype and *Muc13*$^{-/-}$
1027 animals at baseline and after 1 week of stress exposure. Male mice, Two-way ANOVA, n=13 per
1028 group, N=2. (H) DeepLabCut experimental design. (I) Pie chart of quantified behavioral motifs
1029 changed between wildtype and *Muc13*$^{-/-}$ animals. (J) Individual motif analysis after 1 week of
1030 stress exposure between wildtype and *Muc13*$^{-/-}$ animals. Two-tailed T tests, male and female
1031 mice, n=13-24 per group, N=3.
1032

1033 **EXTENDED DATA**

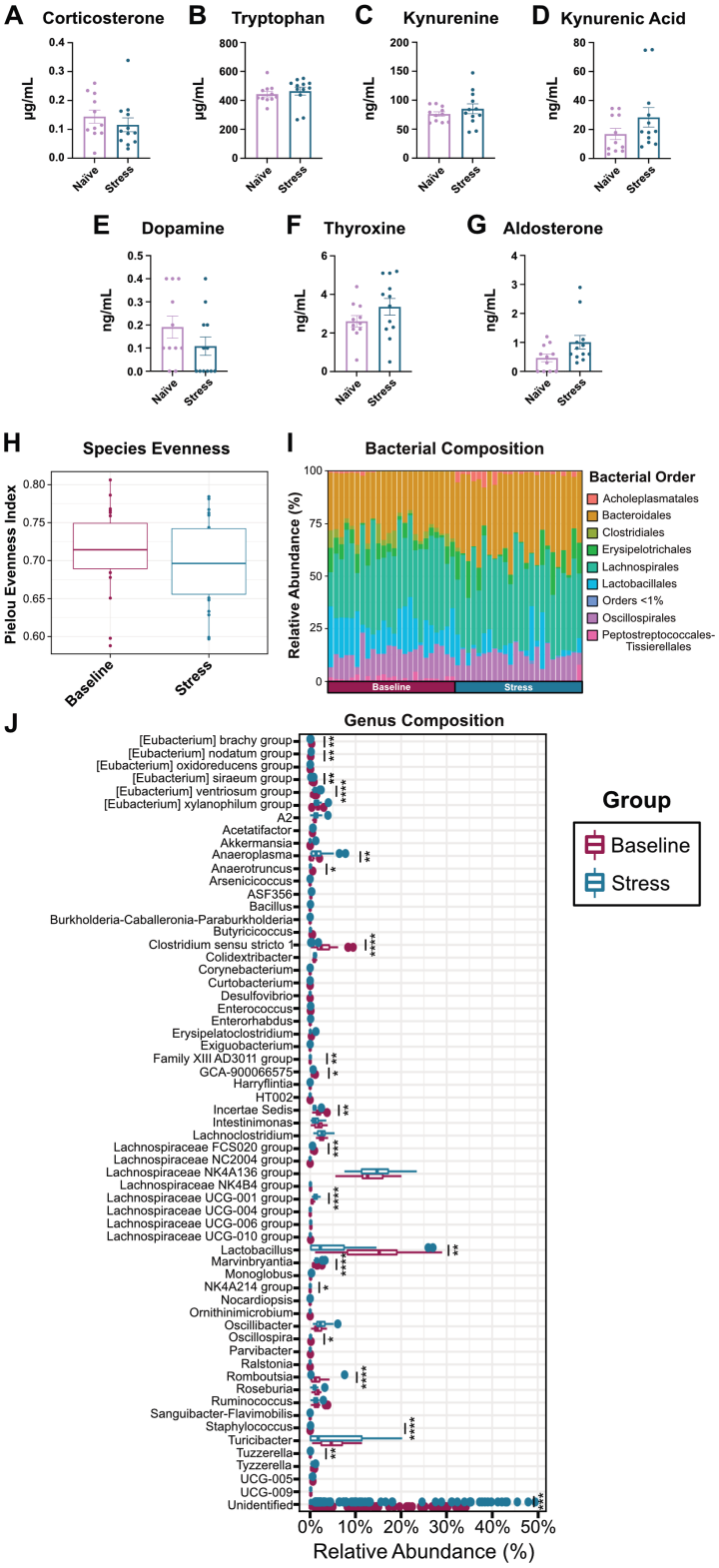

1034

1035 **Extended Data 1: Serum Metabolites and 16S Sequencing after Stress Exposure**: Mass
1036 spectrometry analysis of serum from naïve and stressed mice. (A) corticosterone, (B) tryptophan,
1037 (C) kynurenine, (D) kynurenic acid, (E) dopamine, (F) thyroxine, and (G) aldosterone. Male mice,
1038 n=11/12 per group, N=1, Unpaired two-tailed T-tests. MS Transitions can be found in Ext. Data5,
1039 Tab 1. (H) Pielou's evenness index for baseline and stress mice. (I) Individual order relative
1040 abundances for baseline and stress mice. (J) Relative Abundances of the genus level between
1041 naïve and stress mice. Male mice, n=24/group, N=1. P-values for (J) can be found in Ext. Data 5,
1042 Tab 2.
1043

1044

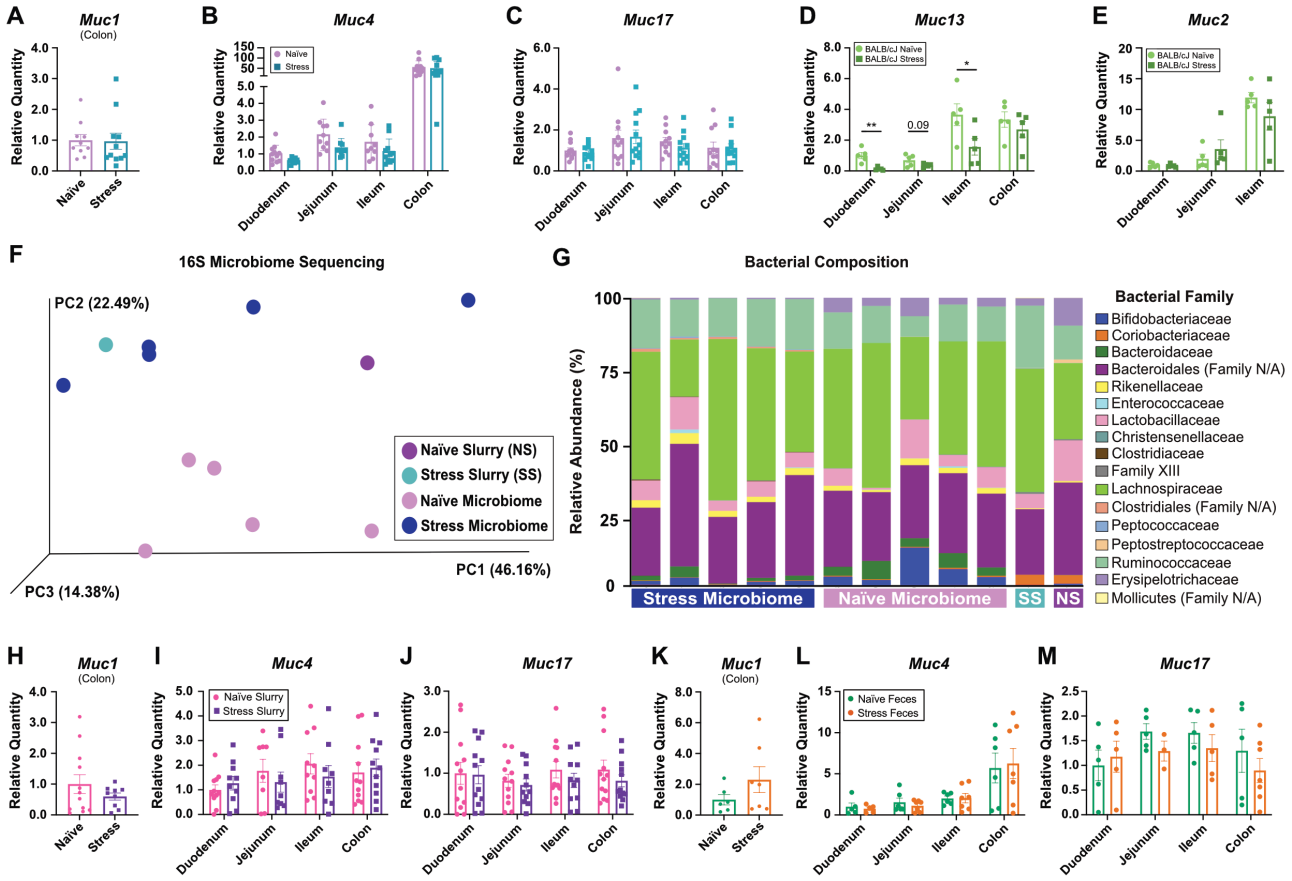

1045

1046 **Extended Data 2: Mucin Expression after Stress and Microbiome Transfers:** (A) Relative quantity
1047 of *Muc1* expression in colon of naïve and stress mice by qPCR. *Muc*1 was not detected in other
1048 sections (two tailed t-test). Relative quantities of (B) *Muc4* and (C) *Muc17* expression in the
1049 intestines of naïve and stress mice by qPCR. Two-way ANOVA (D) Relative quantity of *Muc13* and
1050 (E) *Muc2* expression in sections of the intestines from naïve and stressed male BALB/cJ mice by
1051 qPCR. Two-way ANOVA. Male mice. Experiments A-C, n=11/12 per group. Experiments D-E, n=5
1052 per group. N=1. (F) 16S PCoA plot between naïve and stress slurries and naïve and stress
1053 microbiome recipients. (G) Individual bacterial family compositions. Male mice, n=5/group, slurry
1054 samples from gavage microbiome mixture, N=1. Relative quantities of (H) *Muc1*, (I) *Muc4*, and (J)

1055 *Muc17* from the intestines of mice treated with antibiotics then given naïve or stress fecal slurry.

1056 Male mice, 12/group, N=1, Two-way ANOVA. Relative quantities of (K) *Muc1*, (L) *Muc4*, and (M)

1057 *Muc17* in germ free mice given naïve or stress feces. Male mice, 7/group, N=1, Two-way ANOVA.

1058

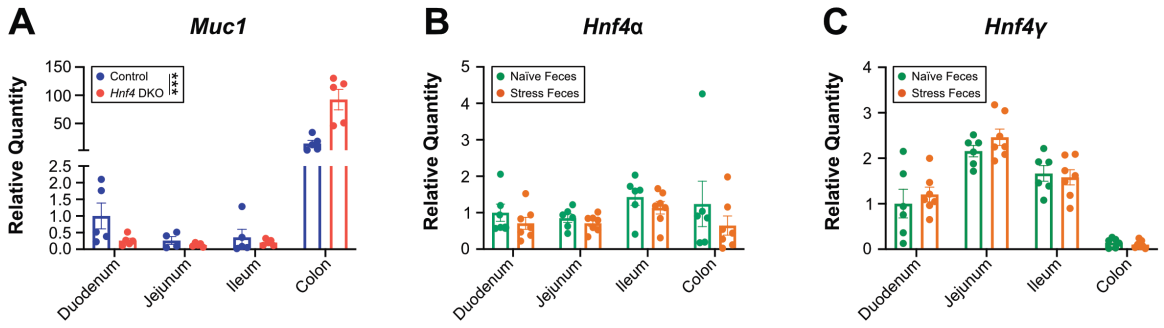

1059

1060 **Extended Data 3: HNF4 Regulates Mucins Independently of Transferrable Microbial Products**.

1061 Relative quantities of (A) *Muc1* in the intestines of *Hnf4* DKO mice. Female mice, 5/group. Two-

1062 way ANOVA. Relative quantities of (B) *Hnf4*α and (C) *Hnf4*γ in the intestines of germ-free mice

1063 given stress or naïve feces. Male mice, 7/group. Two-way ANOVA.

1064

1065

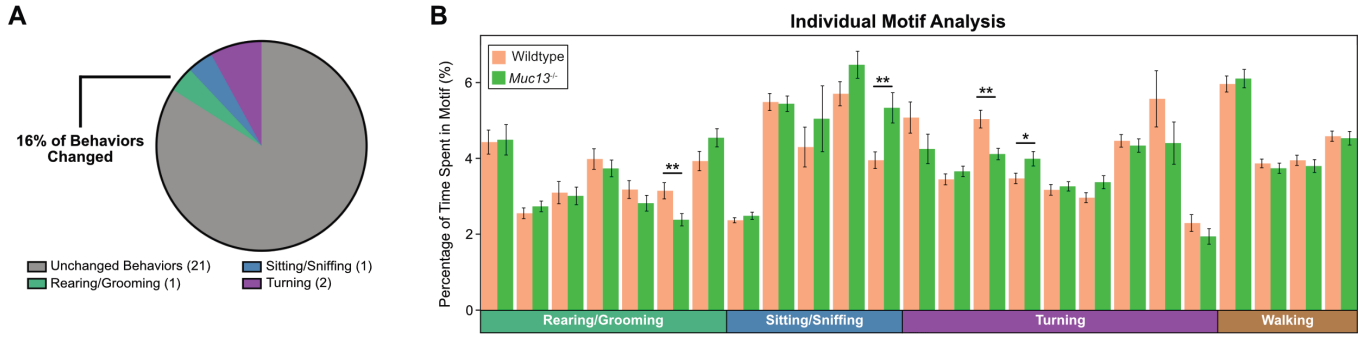

1066

1067 **Extended Data 4: DeepLabCut Analysis of Baseline Behaviors:** (A) Pie chart representing

1068 quantified behavioral motifs changed between wildtype and *Muc13*$^{-/-}$ animals. (B) Individual

1069 motif analysis comparing baseline behaviors in wildtype and *Muc13*$^{-/-}$ animals. Two tailed t-tests,

1070 male and female mice, n=13-24 per group, representative of 3 experiments.

1071

1072

1073 **Extended Data 5: Data Tables:** (1-MS Transitions): Table of mass over charge number (m/z) for
1074 analytes examined between naïve and stressed animals. (2-NaivevStress_Genus_WilcoxRank):
1075 Table of naïve vs stress genus level Wilcox Rank Sum statistics (for Ext. Data 1J). (3-
1076 ASV+Genus_ControltoMuc13KO): Table of statistics for ASV and Genus level changes between
1077 baseline control, baseline *Muc13*$^{-/-}$, 1wk UCMRS control, 1wk UCMRS *Muc13*$^{-/-}$ animals. (4-qPCR
1078 Probes): Table of qPCR probes used in manuscript. (5-Statistics Table): Table of statistics for all
1079 data in manuscript.